

Dalton Transactions

Accepted Manuscript



This is an *Accepted Manuscript*, which has been through the Royal Society of Chemistry peer review process and has been accepted for publication.

Accepted Manuscripts are published online shortly after acceptance, before technical editing, formatting and proof reading. Using this free service, authors can make their results available to the community, in citable form, before we publish the edited article. We will replace this *Accepted Manuscript* with the edited and formatted *Advance Article* as soon as it is available.

You can find more information about *Accepted Manuscripts* in the [Information for Authors](#).

Please note that technical editing may introduce minor changes to the text and/or graphics, which may alter content. The journal's standard [Terms & Conditions](#) and the [Ethical guidelines](#) still apply. In no event shall the Royal Society of Chemistry be held responsible for any errors or omissions in this *Accepted Manuscript* or any consequences arising from the use of any information it contains.

ARTICLE

Tetratopic Pyrimidine-Hydrazone Ligands Modified with Terminal Hydroxymethyl and Acryloyl Arms and their Pb(II), Zn(II), Cu(II) and Ag(I) Complexes

Cite this: DOI: 10.1039/x0xx00000x

Daniel J. Hutchinson, Lyall R. Hanton* and Stephen C. Moratti

Received 00th January 2012,
Accepted 00th January 2012

DOI: 10.1039/x0xx00000x

www.rsc.org/

The first tetratopic pyrimidine-hydrazone (pym-hyz) molecular strands containing terminal hydroxymethyl (**L1**) and acryloyl (**L2**) functional groups have been synthesised. **L1** was produced by step-wise imine condensation reactions, starting with 6-hydroxymethyl-2-pyridinecarboxaldehyde. **L2** was then synthesised through the treatment of **L1** with acryloyl chloride. NMR spectroscopy and X-ray crystallography showed that the ligands adopted a helical shape, comprised of 1 and 1/3 helical turns. Both **L1** and **L2** uncoiled upon reaction with an excess amount of Pb(II), Zn(II) and Cu(II) ions, resulting in linear $M_4L_8A_8$ complexes (where M = Pb(II), Zn(II), or Cu(II); L = **L1** or **L2**; and A = ClO_4^- , $SO_3CF_3^-$ or BF_4^-). Horse-shoe shaped Pb_2LA_4 complexes were also formed by reacting Pb(II) ions with either **L1** or **L2** in a 2:1 metal to ligand ratio. The addition of Ag(I) ions to either **L1** or **L2** resulted in $Ag_2L_2A_2$ double helicates, which were stable in the presence of excess Ag(I). The Pb(II), Zn(II) and Ag(I) complexes were characterised by NMR spectroscopy, while UV-Vis spectroscopy was used to probe the Cu(II) complexes. In addition, X-ray crystallography was used to analyse the linear $Pb_4L_1A_8$, horse-shoe $Pb_2L_1(ClO_4)_4$, twisted $Cu_3L_2(SO_3CF_3)_6$, and double helicate $Ag_2L_1_2(SO_3CF_3)_2$ complexes yielding the structures $[Pb_4L_1(ClO_4)_7(H_2O)]ClO_4 \cdot 4CH_3NO_2$ (**1**), $[Pb_4L_1(SO_3CF_3)_8]_2 \cdot 6CH_3CN \cdot H_2O$ (**2**), $[Pb_2L_1(ClO_4)_2(CH_3CN)(H_2O)](ClO_4)_2 \cdot 2CH_3CN \cdot C_4H_{10}O \cdot H_2O$ (**3**), $[Cu_3L_2(SO_3CF_3)_3(CH_3CN)_2(H_2O)](SO_3CF_3)_3 \cdot 2CH_3CN \cdot H_2O$ (**4**) and $[Ag_2L_1_2(SO_3CF_3)_2 \cdot CH_3CN \cdot H_2O$ (**5**), respectively.

Introduction

The construction of molecular machines which mimic the motions demonstrated by nature's vast array of nanoscale machinery continues to be one of the many challenges facing chemists.¹ Biomolecules such as myosin² have been a source of inspiration, leading to the design of synthetic actuating molecules that exhibit reversible expansion and contraction motions in response to an external stimulus.³ To this end, molecular strands of repeating pyrimidine-hydrazone (pym-hyz) units have been studied due to their molecular actuating behaviour.⁴ The strong preference of the pym-hyz linkage for a transoid conformation⁵ results in the folding of the molecular

strand into a helix,⁶⁻⁸ which is then uncoiled to form a linear strand upon the metal ion induced isomerisation of the pym-hyz linkages in their cisoid conformation.^{4,9} The strands therefore exhibit nanomechanical action, akin to a two-stroke linear motor, stimulated by the reversible binding of metal ions.⁴

While artificial molecular actuator systems, such as the pym-hyz molecular strands, have been developed, their usefulness in performing tasks on a macroscopic scale has yet to be realised.¹⁰ One strategy for harnessing molecular scale motions for macroscopic tasks requires the assembly of molecular actuators into larger integrated systems,¹¹ such as polymer gel actuators. These gels are capable of significant volume and shape changes upon the incidence of a wide range of external stimuli,¹² and consequently have potential applications in the realms of soft robotics¹³ and microfluidics.¹⁴

Our research is focused on creating a polymer gel actuator containing pym-hyz strands which would act as an artificial muscle; expanding and contracting due to the coordination of metal ion guest molecules in the solution phase to the pym-hyz host molecules within the gel network. The incorporation of pym-hyz strands into a gel first requires that functional groups capable of undergoing polymerisation with a co-monomer be appended to the strands. So far we have synthesised and studied ditopic pym-hyz strands with terminal hydroxymethyl¹⁵⁻¹⁷ and

Department of Chemistry, University of Otago, PO Box 56, Dunedin, New Zealand. Email: lhanton@chemistry.otago.ac.nz

† Electronic Supplementary Information (ESI) available: Crystallographic data for **AB**, **L1** and **1-5** including a discussion of how disorder was handled, pictorial views with thermal ellipsoids at the 50 % probability level and selected bond lengths and angles in tabulated form. CCDC reference numbers #####-#####. See DOI: 10.1039/b000000x/

acryloyl¹⁸ arms which uncoil to form linear complexes when reacted with excess Cu(II), Pb(II), Zn(II) and Ag(I) ions. The amplitude of extension, however, is minimal as the ditopic ligands only contain two hyz functions and therefore only represent two thirds of a helical turn.¹⁷ Three hyz functions are required to form a whole helical turn and the extension amplitude of pym-hyz strands has been shown to increase with increasing strand length.^{4,7}

Therefore, we have synthesised and characterised two new tetratopic pym-hyz strands containing terminal hydroxymethyl (**L1**) and acryloyl (**L2**) arms (Scheme 1). These ligands contained four hyz functions and therefore existed as 1 and 1/3 helical turns. While examples of tetratopic pym-hyz strands exist in the literature^{4,7,19} they do not contain groups appended to their terminal pyridine (py) rings. Furthermore, to date, the coordination chemistry of tetratopic pym-hyz strands has only been studied with respect to Pb(SO₃CF₃)₂.⁴ In those studies an excess amount of Pb(II) ions resulted in the uncoiling of the tetratopic ligand to form linear complexes, while a [4x4] grid complex was formed by employing a metal to ligand ratio of 2:1. A tetratopic strand composed of pym-py units, which are known to be isostructural to pym-hyz units,^{4,6,7} has also been reacted with Pb(SO₃CF₃)₂²⁰ and AgSO₃CF₃²¹ in CH₃CN, resulting in various grid complexes and double helicates, respectively.

Previous studies carried out in our research group have shown that the addition of terminal hydroxymethyl and acryloyl arms to ditopic pym-hyz ligands affects the outcome of self-assembly at low metal to ligand ratios as these groups crowd the bound metal ions in both a steric and coordinative fashion.¹⁵⁻¹⁸ The extent to which the supramolecular structure is affected by the additional groups is dependent on the size of metal ion, as well as the counteranion of the metal salt and even the choice of solvent.

Therefore we endeavoured to investigate the interactions of **L1** and **L2** with Pb(II), Zn(II), Cu(II) and Ag(I) salts in both CH₃CN and CH₃NO₂ at a variety of metal to ligand ratios. It was discovered that linear M₄L₈ complexes (where M = Pb(II), Zn(II), or Cu(II); L = **L1** or **L2**; and A = ClO₄⁻, SO₃CF₃⁻ or BF₄⁻) could be synthesised through reacting **L1** or **L2** with an excess quantity of Pb(II), Zn(II) or Cu(II) ions, while the only complexes that could be synthesised with Ag(I) ions were Ag₂L₂A₂ double helicates. The formation of Ag₂L₂A₂ double helicates was unexpected since the steric bulk of the acryloyl arms prevented their formation with the modified ditopic pym-hyz ligand.¹⁸ The addition of Pb(II) ions to **L1** or **L2** in a 2:1 metal to ligand ratio resulted in horse-shoe shaped Pb₂L₄ complexes as opposed to [4x4] grids. A twisted Cu₃L₂(SO₃CF₃)₆ was also crystallised from a solution of the linear Cu₄L₂(SO₃CF₃)₈ complex. Herein we report the synthesis and characterisation of these two new tetratopic ligands and the solution phase and solid state structures of their various complexes.

Results and Discussion

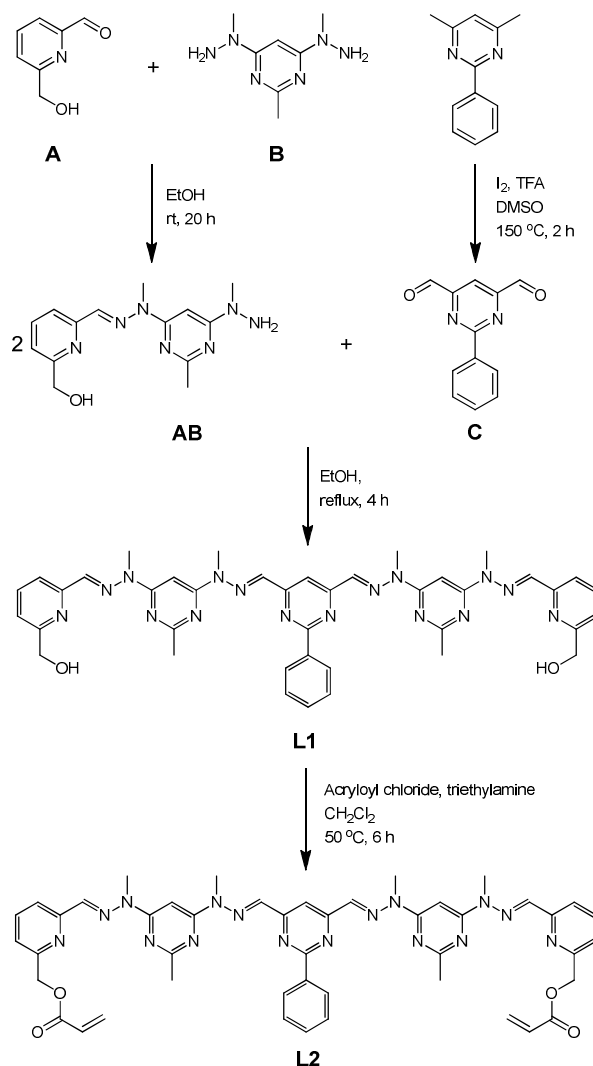
Organic Synthesis

The tetratopic, hydroxymethyl terminated ligand **L1** was synthesised through a double condensation reaction between 6-hydroxymethyl-2-pyridinecarboxaldehyde, 2-methyl-2-[6-(1-methylhydrazinyl)-4-pyrimidinyl]hydrazine (**AB**) and 2-phenyl-4,6-pyrimidinedicarboxaldehyde (**C**) in a 2:1 molar ratio. The ligand was then reacted with acryloyl chloride in the

presence of triethylamine²² to convert the terminal hydroxymethyl arms into acryloyl arms, producing ligand **L2** (Scheme 1).

AB was first synthesised by reacting 6-hydroxymethyl-2-pyridinecarboxaldehyde (**A**) and 4,6-bis(1-methylhydrazino)-2-methylpyrimidine (**B**) in a 1:1 molar ratio in EtOH. The double condensation reaction, which would have produced the undesired ditopic ligand,⁷ was avoided by adding a dilute solution of **A** dropwise to a concentrated solution of **B**, in order to maintain the molar excess of **B** in solution, and by performing the reaction at room temperature. The low solubility of **AB** in EtOH at room temperature meant that it was precipitated from the solution as a pure white solid in high yields of 80 to 90 %.

The white precipitate produced microanalytical results consistent with the formula of **AB**·1/2H₂O. The ESMS spectrum showed peaks due to the [AB+Na]⁺ and [AB+H]⁺ molecular ions. The IR spectrum showed a C=N stretching mode at 1566 cm⁻¹, confirming the formation of the imine bond between **A**



Scheme 1. The synthetic strategy employed to produce **L1** and **L2**.

and **B**. A broad O-H stretching mode at 3167 cm^{-1} and a N-H stretching mode at 3332 cm^{-1} indicated the presence of the hydroxymethyl arm and hydrazine functional groups of **AB**. The transoid-transoid conformation of the pym-hyz-py bond of **AB** was evident from the lack of correlations between H5 and H9, and H10 and H12 in the 2D NOESY NMR spectrum. The solution phase conformation was consistent with the solid state structure of **AB**, determined from X-ray analysis of crystals grown by the slow evaporation of the CDCl_3 NMR solution (Figure 1). The hydroxymethyl arms were involved in self-complementary, intermolecular H-bonding which linked adjacent molecules of **AB** together as dimers. The O1-H1...N1 distance was $2.203(3)\text{ \AA}$, corresponding to an O1...N1 distance of $2.836(3)\text{ \AA}$ (Figure 2).

AB was then refluxed with **C** in a 2:1 molar ratio in EtOH, resulting in the formation of **L1**, which precipitated from the solution as a pure white solid in high yields of between 80 and 85 % (Scheme 1). The microanalytical results from this solid matched the formula of $\text{L1}\cdot\text{H}_2\text{O}$. The molecular ions $[\text{L1}+\text{Na}]^+$ and $[\text{L1}+\text{H}]^+$ were identified in the ESMS spectrum. The O-H and C=N stretching modes gave peaks in the IR spectrum at 3373 and 1559 cm^{-1} , respectively. The 2D NOESY NMR spectrum showed that the molecule adopted a helical shape with transoid pym-hyz and hyz-py bonds (Figure 3). The H5 and H14 signals occurred in the ^1H NMR spectrum at 8.49 and 7.31 ppm, respectively, due to deshielding from the adjacent transoid pym-hyz linkages.⁷ The folding of **L1** into a helix also resulted in shielding of the terminal py protons, resulting in their signals appearing at lower chemical shifts than in the ^1H NMR spectrum of the non-helical ditopic hydroxymethyl terminated pym-hyz strand.¹⁷

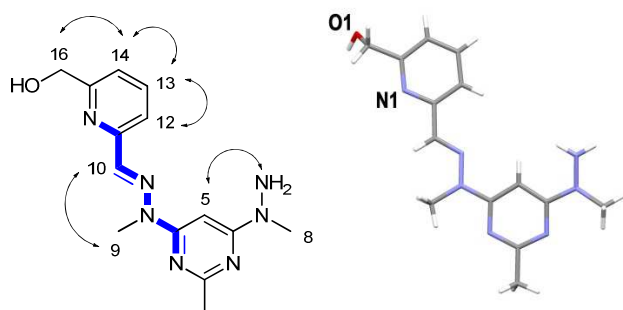


Figure 1. The (left) solution phase structure of **AB** showing the NOE correlations seen in the 2D NOESY spectrum (NMR numbering) and (right) the solid state structure of **AB** (crystallographic numbering).

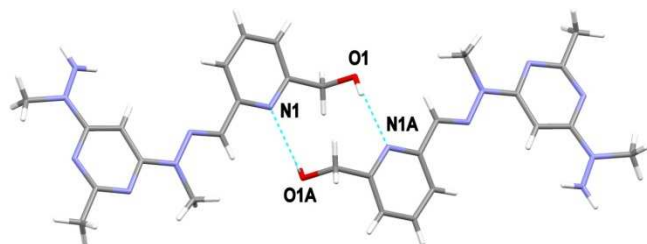


Figure 2. View of two molecules of **AB** organised as dimers due to self complementary intermolecular H-bonding between O1 and N1 (symmetry codes A: 1-x, 1-y, 1-z).

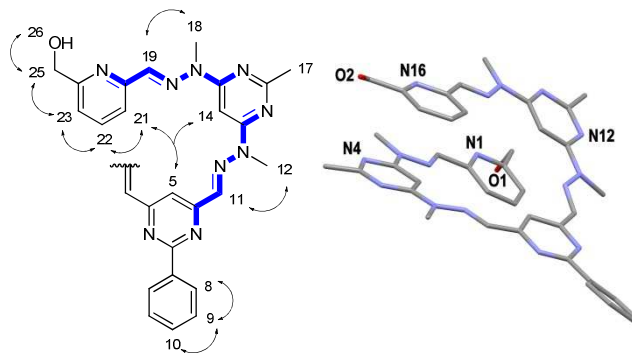


Figure 3. The (left) solution phase structure of **L1** showing the NOE correlations seen in the 2D NOESY spectrum (NMR numbering) and (right) the solid state structure of **L1** (crystallographic numbering; hydrogens removed for clarity).

Crystals of **L1** were grown by the slow diffusion of diethyl ether into a CH_2Cl_2 solution of the ligand. The solid state structure of these crystals was that of a helix with $1\text{ and } \frac{1}{3}$ turns (Figure 3), a helical pitch of 3.6 \AA , and a length of 3.9 \AA (measured from the centroid of the N1 py ring to the mean plane of the N16 py ring). The helix was stabilised by π - π stacking interactions between the overlapping py and pym rings [centroid to centroid distances of $3.504(5)$ and $3.545(6)$ for the N1 py ring to the N12 pym ring, and the N16 py ring to the N4 pym ring, respectively]. The added hydroxymethyl arms resulted in the aggregation of **L1** into quartets of molecules through intermolecular H-bonding between O1 and N1, and O2 and N16, with O1-H1...N1 and O2-H2...N16 distances of $2.343(10)$ and $2.074(12)\text{ \AA}$, respectively [corresponding to O1...N1 and O2...N16 distances of $2.762(9)$ and $2.813(10)\text{ \AA}$, respectively; Figure 4].

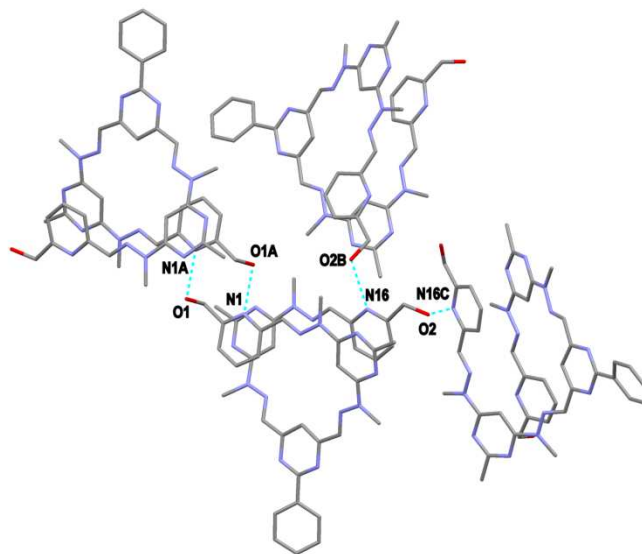


Figure 4. View of the H-bonding which links one molecule of **L1** to three others (hydrogens omitted for clarity; symmetry codes A: $\frac{1}{2}$ -x, $-\frac{1}{2}$ -y, $\frac{1}{2}$ -z; B: $-\frac{3}{4}$ +x, $\frac{1}{4}$ -y, 1.25 -z; C: $\frac{1}{4}$ -x, $\frac{3}{4}$ +y, 1.25 -z).

The hydroxymethyl arms of **L1** were converted into acryloyl groups by reacting **L1** with an excess quantity of acryloyl chloride in the presence of triethylamine.²² The limited solubility of **L1** in CH₂Cl₂ required that the reaction be carried out at 50 °C. Following the removal of excess acrylic acid and protonated triethylamine with aqueous washings, **L2** was isolated as a crude brown solid residue. Washing this residue with acetone resulted in **L2** as a pure off-white solid, the microanalytical results of which were consistent with the formula for **L2**. The ESMS spectrum showed a peak corresponding to the [L₂+Na]⁺ molecular ion. The IR spectrum showed C=O and C=N stretching modes at 1728 and 1561 cm⁻¹, respectively. The ¹H NMR spectrum of **L2** was very similar to that of **L1**, with the exception of the extra acryloyl proton signals which occurred as a series of double doublets between 5.92 and 6.54 ppm. The NOE correlations of **L2** showed it also adopted a helical shape in solution with transoid pym-hyz and py-hyz bonds, analogous to **L1** (Figure 3).

Synthesis and Structures of L1 and L2 Complexes

The coordination chemistry of tetratopic pym-hyz strands has previously only been probed by reactions with Pb(SO₃CF₃)₂ in CH₃CN.⁴ In those studies a 2:1 metal to ligand ratio resulted in [4x4] grid complexes, while a 4:1 ratio led to linear complexes. In this study, ligands **L1** and **L2** were reacted with salts of Pb(II), Zn(II), Cu(II) and Ag(I) in either CH₃CN or CH₃NO₂. Solutions of the metal salts were added to the ligands at elevated temperatures, resulting in dissolution of the ligand upon complexation. In contrast to the behaviour of the previously investigated hydroxymethyl and acryloyl terminated ditopic ligands,^{15, 16, 18} the outcomes of the reactions with **L1** and **L2** were not influenced by the choice of solvent. As a result CH₃CN was the solvent primarily used to produce complexes for analysis. Reacting the tetratopic ligands with an excess of Pb(ClO₄)₂·3H₂O, Pb(SO₃CF₃)₂·H₂O, Zn(SO₃CF₃)₂, Cu(ClO₄)₂·6H₂O or Cu(SO₃CF₃)₂·4H₂O resulted in linear complexes of type M₄LA₈ (where M = Pb(II), Zn(II), or Cu(II); L = **L1** or **L2**; and A = ClO₄⁻, SO₃CF₃⁻ or BF₄⁻). Horse-shoe shaped Pb₂LA₄ complexes were formed by reacting **L1** or **L2** with Pb(II) ions in a 2:1 metal to ligand ratio, while the only complexes formed through reacting the ligands with AgSO₃CF₃ or AgBF₄ were Ag₂L₂A₂ double helicates (Figure 5).

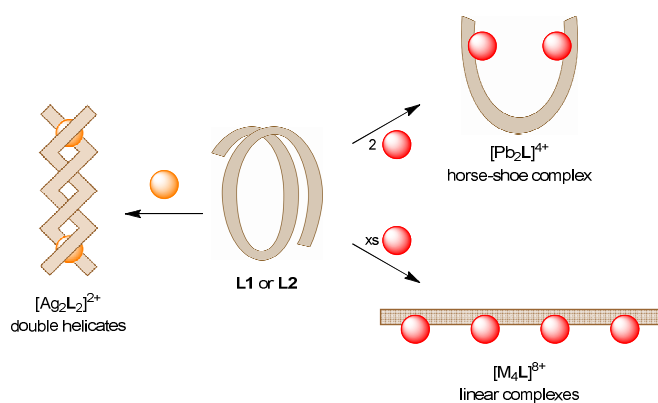


Figure 5. Summary of the metal complexes formed from **L1** and **L2** (where M = Pb(II), Zn(II), or Cu(II); L = **L1** or **L2**; and A = ClO₄⁻, SO₃CF₃⁻ or BF₄⁻).

The metal to ligand ratios required to achieve complete conversion of the ligands to the linear complexes differed depending on the metal ion employed. Complete dissolution of **L1** and **L2** was achieved with either Pb(II) salt at a metal to ligand ratio of 2:1, however a 4:1 ratio was required for the synthesis of the linear Pb₄LA₈ complexes. A ratio of 4:1 was necessary for complete dissolution of the ligands when using Zn(SO₃CF₃)₂, at which point the solution contained a mixture of complexes. A ratio of 10:1 was needed for the exclusive formation of the linear Zn₄L(SO₃CF₃)₈ complexes. The ligands were also reacted with Zn(BF₄)₂, however complete dissolution was not achieved at any metal to ligand ratio. Reacting either of the ligands with the Cu(II) salts resulted in complete dissolution and the formation of Cu₄LA₈ complexes at a 4:1 metal to ligand ratio, however, attempts to crystallise the Cu₄L₂(SO₃CF₃)₈ complex resulted in crystals of a **L2** complex coordinated with only three Cu(II) ions. This suggested an equilibrium process in which Cu(II) ions were exchanged between the Cu₄L₂(SO₃CF₃)₈ complex and the CH₃CN solvent. The Ag(I) salts only required a 1:1 metal to ligand ratio to completely convert **L1** or **L2** into the Ag₂L₂A₂ double helicates. Addition of excess Ag(I) to these complexes had no effect on the composition of the solutions.

Analysis of L1 and L2 Complexes. The CH₃CN solutions were stirred with diethyl ether, resulting in the precipitation of the complexes as powders, which were then isolated by filtration and dried in vacuo. In the cases of the Pb(II), Zn(II) and Cu(II) complexes the microanalytical results from the solids supported the expected formula, however the results showed several of the complexes were hydrated or solvated with CH₃CN. The microanalytical results from the Ag₂L₂A₂ complexes indicated that their solid precipitates also contained small portions of uncoordinated AgSO₃CF₃ and AgBF₄, despite extensive washings with diethyl ether.

The ESMS spectra of the complexes typically only showed a peak due to either of the [L+Na]⁺ molecular ions, however, the spectrum of the Pb₄L₁(ClO₄)₈ complex also showed peaks due to the [Pb₂L₁(ClO₄)₃]⁺ and [Pb₂L₁-2H]²⁺ molecular ions. Additional peaks in the spectra of the Zn₄L₁(SO₃CF₃)₈ and Cu₄L₁(ClO₄)₈ complexes were due to the [Zn₂L₁(SO₃CF₃)₃]⁺, [Zn₂L₁(SO₃CF₃)₂]²⁺, [CuL₁(ClO₄)]⁺ and [Cu₂L₁-2H]²⁺ molecular ions. The ESMS spectra of the Ag(I) complexes of **L1** and **L2** all showed peaks due to the [AgL]⁺ molecular ions, while the Ag₂L₁2(SO₃CF₃)₂ complex also showed peaks due to the [Ag₂L₁2(SO₃CF₃)]⁺ and [Ag₂L₁(SO₃CF₃)]⁺ ions.

The IR spectra of the **L1** complexes showed that the coordination of Pb(II) and Ag(I) ions to **L1** shifted the C=N stretching mode from 1559 cm⁻¹ to between 1551 and 1541 cm⁻¹. In contrast, the coordination of Zn(II) and Cu(II) ions barely affected the frequency of the **L1** C=N stretching mode, which occurred between 1559 and 1556 cm⁻¹. All of the complexes of **L2** showed a decrease in frequency of the C=N stretching mode from 1561 cm⁻¹ to between 1556 and 1540 cm⁻¹. The Pb(II) and Cu(II) complexes of **L2** also showed a decrease in frequency of the C=O stretching mode from 1728 cm⁻¹ to between 1720 and 1707 cm⁻¹. The coordination of metal ions to **L1** did not have a unified effect on the O-H stretching mode, with the frequencies ranging between 3505 and 3357 cm⁻¹. All of the complexes showed stretching modes due to their ClO₄⁻, SO₃CF₃⁻ or BF₄⁻ counterions between 1047 and 1052, 1272 and 1211, and 1039 and 1037 cm⁻¹, respectively.

The Cu(II) complexes of **L1** and **L2** were also analysed by UV-Vis spectroscopy, with each of their spectra showing a single broad d-d transition with a λ_{max} of either 690 or 691 nm

for the $\text{Cu}_4\text{L1}(\text{ClO}_4)_8$ and $\text{Cu}_4\text{L1}(\text{SO}_3\text{CF}_3)_8$ complexes, or 684 or 687 nm for the $\text{Cu}_4\text{L2}(\text{ClO}_4)_8$ and $\text{Cu}_4\text{L2}(\text{SO}_3\text{CF}_3)_8$ complexes, respectively. The wavelengths of these transitions were consistent with Cu(II) ions surrounded by N donors in either distorted trigonal bipyramidal or distorted octahedral environments.²³ Their extinction coefficients of 449, 417, 546 and 508 $\text{L mol}^{-1} \text{cm}^{-1}$, respectively, were roughly twice the values of the d-d transitions recorded for the linear Cu(II) complexes of the hydroxymethyl¹⁷ and acryloyl¹⁸ terminated ditopic pym-hyz ligands.

NMR Spectroscopy of L1 and L2 Complexes. ^1H and 2D ROESY NMR spectroscopy showed that the Pb_4LA_8 and $\text{Zn}_4\text{L}(\text{SO}_3\text{CF}_3)_8$ complexes were linear in shape, with cisoid pym-hyz and hyz-py linkages and metal ions occupying each of the coordination pockets (Figure 6). The uncoiling of the L1 and L2 ligands upon the coordination of Pb(II) or Zn(II) ions resulted in several distinctive changes to the ^1H NMR spectrum. The rotation of the pym-hyz linkages from transoid to cisoid caused upfield shifts in the positions of the H5 and H14 pym signals.⁴ The binding of metal ions to coordination sites resulted in downfield shifts for the hyz and py proton signals. The latter were further shifted downfield due to the removal of shielding π - π stacking interactions upon the uncoiling of the ligand strands.⁴ Based on the downfield shift of the hydroxymethyl signals of L1, and the lack of movement of the acryloyl arm signals of L2, upon the formation of the linear complexes, it appeared that the hydroxymethyl arms were coordinated to the terminal Pb(II) and Zn(II) ions while the acryloyl arms were not. This coordinative behavior was identical to that of the ditopic hydroxymethyl and acryloyl ditopic pym-hyz strands.^{16, 18}

Several of the proton signals in the ^1H NMR spectra of the Pb_4LA_8 complexes were significantly broadened when a metal to ligand ratio of 4:1 was employed, indicating that the linear complexes were rapidly exchanging with other complex species in solution. The broadened signals originated from the pym and hyz protons surrounding the innermost pym-hyz-pym coordination pockets, and the protons of the phenyl ring on the central pym, which suggested that the Pb(II) ions in these

coordination pockets were more labile than those in the terminal pym-hyz-py pockets. Decreasing the temperature from 298 to 243 K allowed for the resolution of the different complex signals. Increasing the metal to ligand ratio sharpened the signals significantly as the excess ions shifted the equilibrium further towards the linear Pb_4LA_8 species (Figure 7). In contrast, the addition of $\text{Zn}(\text{SO}_3\text{CF}_3)_2$ to L1 or L2 in a 4:1 metal to ligand ratio resulted in a complicated ^1H NMR spectra showing multiple complexes slowly exchanging in solution. Increasing the metal to ligand ratio to 10:1 resulted in a dramatic simplification of the spectra as the multiple species in solution were converted to the linear $\text{Zn}_4\text{L}(\text{SO}_3\text{CF}_3)_8$ complexes.

The ROESY spectra of the Pb_2LA_4 complexes showed they consisted of a horse shoe shaped ligand backbone with Pb(II) ions occupying the terminal pym-hyz-py coordination sites. As a result these sites adopted cisoid-cisoid conformation, while the vacant pym-hyz-pym sites retained their transoid-transoid conformations (Figure 6). The chemical shifts of the H5 and H14 pym signals were similar to the native ligands due to the incomplete isomerisation of the pym-hyz bonds in the Pb_2LA_4 complexes. The partial unfolding of the ligand removed the π - π interactions between the heterocyclic rings, resulting in a downfield shift of the py signals. The selective binding of the Pb(II) ions to the terminal coordination sites also resulted in downfield shifts to the H19 hyz signals, while the H11 hyz signals occurred at chemical shifts similar to those seen in the spectra of L1 and L2. As with the linear complexes it appeared that the hydroxymethyl arms were coordinated to the Pb(II) ions in the $\text{Pb}_2\text{L1A}_4$ complexes, while the acryloyl arms did not interact with the metal ions in the $\text{Pb}_2\text{L2A}_4$ complexes.

The ^1H NMR spectra of the Ag(I) and L1 or L2 solutions showed that the $\text{Ag}_2\text{L}_2\text{A}_2$ double helicates were the only species present at all metal to ligand ratios from 1:1 and above. The coordination of the Ag(I) ions to the py and hyz N donors of the terminal coordination sites resulted in the hyz-py bonds adopting a cisoid conformation and the pym-hyz bonds retaining their transoid conformations (Figure 6). The selective binding of Ag(I) ions towards the more basic py N donors, at

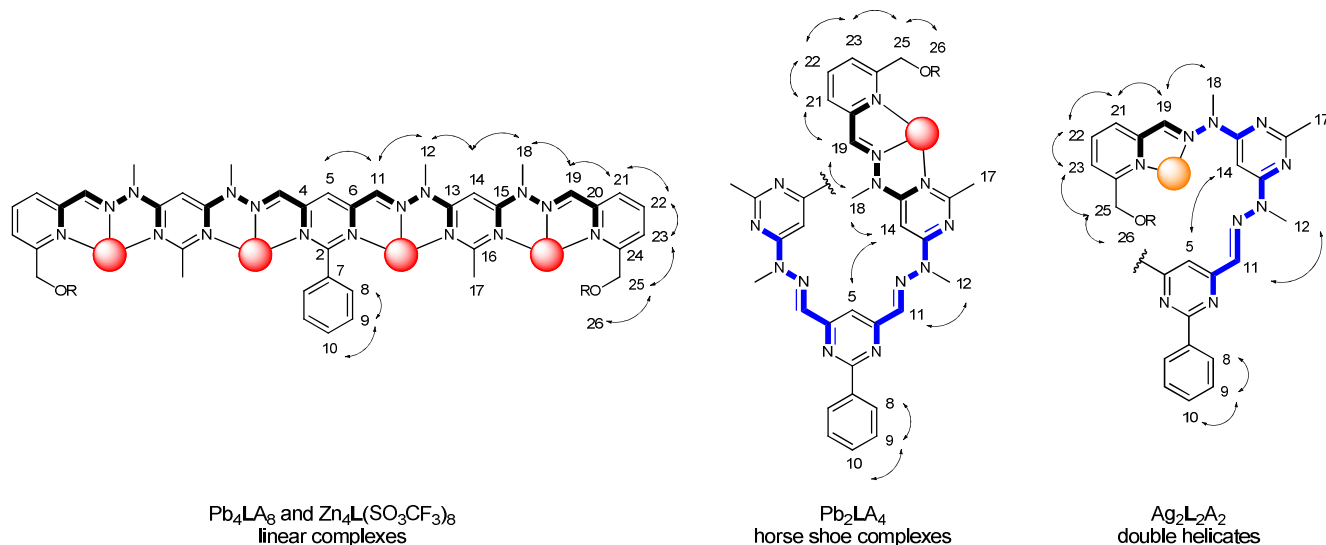


Figure 6. The solution phase conformations of the Pb(II), Zn(II) and Ag(I) complexes of L1 and L2 as deduced from NMR spectroscopy, showing their NOE correlations (NMR numbering; transoid and cisoid pym-hyz and hyz-py bonds are highlighted blue or black, respectively).

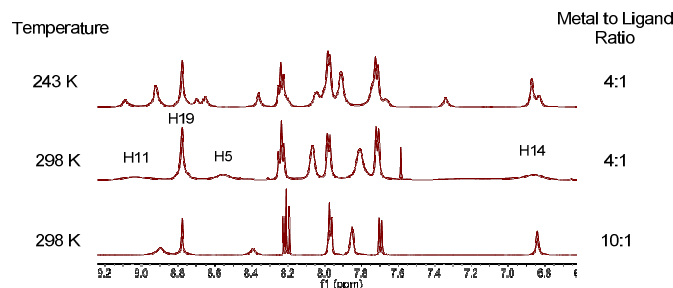


Figure 7. The aromatic region of the ^1H NMR spectra of the $\text{Pb}_4\text{L1}(\text{ClO}_4)_8$ complex at different metal to ligand ratios and temperatures (NMR numbering).

the expense of the pym N donors, was in keeping with their soft classification.^{24, 25} The 2D ROESY spectra showed that the H5 and H14 pym signals were orientated towards each other in the interior of the helicate. The close proximity of the two intertwined **L1** or **L2** molecules resulted in shielding of these protons. The protons from the hydroxymethyl and acryloyl arms were also shielded; however the chemical equivalence of the methylene protons suggested that the arms were able to freely rotate in solution.

X-ray Crystallography of **L1** and **L2** Complexes

Crystals were grown of the linear $\text{Pb}_4\text{L1}(\text{ClO}_4)_8$ and $\text{Pb}_4\text{L1}(\text{SO}_3\text{CF}_3)_8$ complexes through the slow diffusion of diethyl ether into CH_3NO_2 and CH_3CN solutions, respectively, yielding the structures $[\text{Pb}_4\text{L1}(\text{ClO}_4)_7(\text{H}_2\text{O})](\text{ClO}_4) \cdot 4\text{CH}_3\text{NO}_2$ (**1**) and $[\text{Pb}_4\text{L1}(\text{SO}_3\text{CF}_3)_8]_2 \cdot 6\text{CH}_3\text{CN} \cdot \text{H}_2\text{O}$ (**2**). The horse-shoe shaped $\text{Pb}_2\text{L1}(\text{ClO}_4)_4$ complex was crystallised from CH_3CN in a similar fashion, the analysis of which resulted in the structure of $[\text{Pb}_2\text{L1}(\text{ClO}_4)_2(\text{CH}_3\text{CN})(\text{H}_2\text{O})](\text{ClO}_4)_2 \cdot 2\text{CH}_3\text{CN} \cdot \text{C}_4\text{H}_{10}\text{O} \cdot \text{H}_2\text{O}$ (**3**). Attempts to crystallise the $\text{Cu}_4\text{L2}(\text{SO}_3\text{CF}_3)_8$ complex through the diffusion of diethyl ether resulted in crystals of the twisted $[\text{Cu}_3\text{L2}(\text{SO}_3\text{CF}_3)_3(\text{CH}_3\text{CN})_2(\text{H}_2\text{O})](\text{SO}_3\text{CF}_3)_3 \cdot 2\text{CH}_3\text{CN} \cdot \text{H}_2\text{O}$ (**4**) complex instead. The slow diffusion of diethyl ether into a CH_3CN solution of the double helicate $\text{Ag}_2\text{L1}_2(\text{SO}_3\text{CF}_3)_2$ complex yielded crystals of $[\text{Ag}_2\text{L1}_2](\text{SO}_3\text{CF}_3)_2 \cdot \text{CH}_3\text{CN} \cdot \text{H}_2\text{O}$ (**5**).

Complexes **1** and **2** consisted of linear **L1** molecules with cisoid pym-hyz bonds and Pb(II) ions occupying each coordination pocket, similar to the solution phase $\text{Pb}_4\text{L1A}_8$ structures identified by NMR spectroscopy (Figure 8). The length of each complex was 27.8 Å and 28.1 Å, respectively, which when compared to the length of **L1** corresponded to an extension amplitude of 24.2 Å. This value was comparable to that of the unmodified tetrapopic pym-hyz strand reported in the literature upon coordination with $\text{Pb}(\text{SO}_3\text{CF}_3)_2$.⁴ Also similar to that literature complex was the dimeric arrangement of complex **2** due to several of the SO_3CF_3^- anions bridging between the Pb(II) ions bound to neighbouring **L1** molecules (Figure 8). While the two **L1** molecules of **2** were not crystallographically related their bond lengths and angles were equivalent within experimental error. Each of the Pb(II) ions in complexes **1** and **2** were bound to the three N donors of each coordination pocket. The hydroxymethyl arms were consistently coordinated to the Pb(II) ions in the terminal pockets, as was the case with the ditopic hydroxymethyl pym-hyz ligands.¹⁶ The vacancies in the coordination spheres of the Pb(II) ions were satisfied with H_2O molecules, ClO_4^- or SO_3CF_3^- anions, and stereochemically active lone pairs of electrons.²⁶

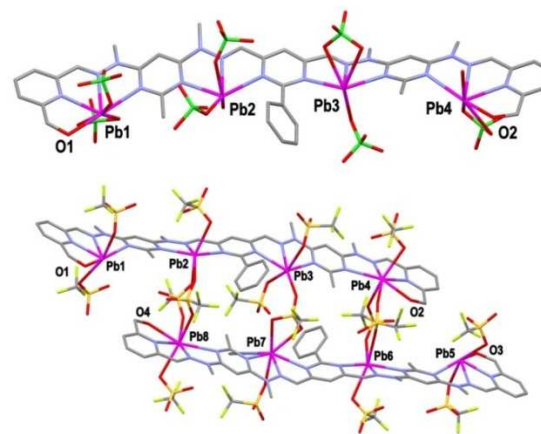


Figure 8. View of the cation molecules of (top) complex **1** and (bottom) complex **2** (hydrogen atoms omitted for clarity; crystallographic numbering).

The structure of complex **3** was also similar to its solution phase analogue as it was a horse-shoe shaped complex with Pb(II) ions bound only in the terminal pym-hyz-py coordination pockets (Figure 9). Complex **3** was therefore vastly different to the [4x4] square grids which were previously the outcome of reacting $\text{Pb}(\text{SO}_3\text{CF}_3)_2$ with tetrapopic pym-hyz⁴ and pym-py²⁰ strands in a 2:1 metal to ligand ratio. Two factors may have contributed to the inability of **L1** to form a grid structure: (i) the steric bulk of the phenyl ring appended to the central pym, and (ii) the crowding of the Pb(II) ions due to the coordination of the hydroxymethyl arms, which may have prevented the ions from binding to more than one **L1** molecule.^{16-18, 27}

Complex **4** was another example of a pym-hyz strand unsaturated with metal ions, as it consisted of three Cu(II) ions occupying three of the four coordination pockets of **L2** (Figure 9). While the pym-hyz bonds coordinated to the Cu(II) ions were rotated to their cisoid conformation, the pym-hyz bond of the vacant pocket retained its transoid conformation. This imparted a twisted shape to complex **4**. The Cu(II) ions were coordinated to the three N donors of each pocket, but not to the terminal acryloyl arms. Each Cu(II) ion existed in a five coordinate distorted square pyramidal environment (τ_5 values of 0.27, 0.07 and 0.21 for Cu1, Cu2, and Cu3, respectively)²⁸ with additional bonds to SO_3CF_3^- anions, CH_3CN or H_2O molecules. Both compounds **3** and **4** were examples of architectures previously unseen for tetrapopic pym-hyz complexes.

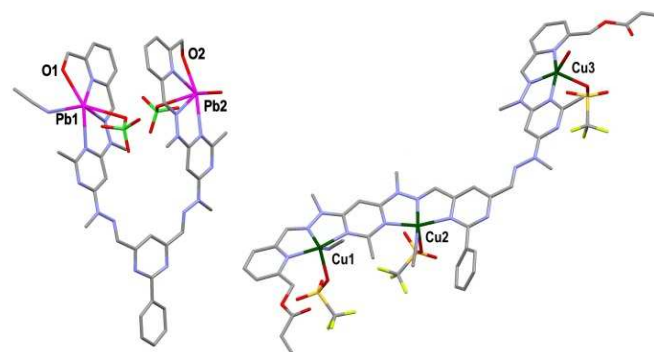


Figure 9. View of the cation molecules of (left) complex **3** and (right) complex **4** (hydrogens omitted for clarity; crystallographic numbering).

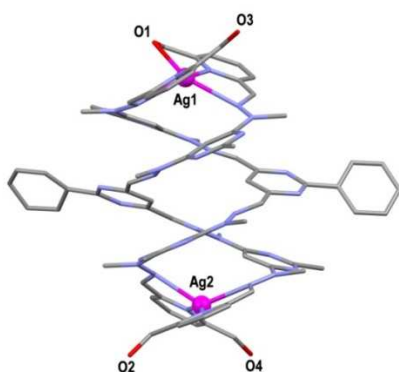


Figure 10. View of the $[Ag_2L1]^{2+}$ cation of complex **5**.

The Ag(I) double helicate complex **5** consisted of two helical **L1** molecules sharing two Ag(I) ions between their terminal pym-hyz-py coordination pockets (Figure 10). The preferential binding of the Ag(I) ions to the hyz and py N donors over the pym N donors, resulted in transoid-cisoid pym-hyz-py bonds and transoid-transoid pym-hyz-pym linkages. Ag1 was also bound to the hydroxymethyl arm of one of the **L1** molecules and resulted in a five coordinate distorted square pyramidal environment ($\tau_5=0.36$).²⁸ In contrast, Ag2 was not bound to either hydroxymethyl arm and existed in a four coordinate, distorted, tetrahedral geometry ($\tau_4=0.52$).²⁹ The resulting asymmetry was the only major deviation of complex **5** from the solution phase $Ag_2L1_2A_2$ structure. The presence of the hydroxymethyl arms also prevented any intermolecular Ag(I)-Ag(I) interactions, which are a common feature of Ag(I) double helicates made from unmodified pym-hyz²⁵ and pym-py²¹ ligands.

Experimental Section

Materials and instrumentations

All starting materials, reagents and metal salts were purchased from commercial sources and were used as received without further purification, with the exceptions of $Pb(SO_3CF_3)_2 \cdot H_2O$ and $Cu(SO_3CF_3)_2 \cdot 4H_2O$ which were produced through the treatment of $2PbCO_3 \cdot Pb(OH)_2$ and $CuCO_3 \cdot Cu(OH)_2 \cdot H_2O$, respectively, with aqueous triflic acid. The precursors 6-hydroxymethyl-2-pyridinecarboxaldehyde (**A**),³⁰ 4,6-bis(1-methylhydrazino)-2-methylpyrimidine (**B**)³¹, 4,6-dimethyl-2-phenylpyrimidine³² and 2-phenyl-4,6-pyrimidinedicarboxaldehyde (**C**)³³ were prepared according to their literature methods. All solvents were used as received, and were of LR grade or better.

Microanalyses were carried out in the Campbell Microanalytical Laboratory, University of Otago. All measured microanalysis results had an uncertainty of $\pm 0.4\%$. 1H and ^{13}C NMR spectra and two dimensional (gCOSY, NOESY, ROSEY, HSQC, gHMBC) spectra were collected on a 500 MHz Varian UNITY INOVA spectrometer at 298 K. Spectra were referenced to the internal solvent signal, with chemical shifts reported in δ units (ppm). Electrospray Mass Spectrometry (ESMS) was carried out on a Bruker microTOFQ instrument (Bruker Daltonics, Bremen, Germany) by employing direct infusion into an ESI source in positive mode. Infrared (IR) spectra were recorded on a Bruker Alpha-P ATR-IR spectrometer. UV-Vis spectra were collected on an Agilent

8453 spectrophotometer against a CH_3CN background using quartz cells with a 1 cm path length.

6-Hydroxymethyl-2-pyridinecarbox-aldehyde, 2-methyl-2-[6-(1-methylhydrazinyl)-4-pyrimidinyl]hydrazone (AB). A solution of 6-hydroxymethyl-2-pyridinecarboxaldehyde (**A**; 2.00 g, 14.6 mmol) in EtOH (300 mL) was added dropwise to a stirring solution of 4,6-bis(1-methylhydrazino)-2-methylpyrimidine (**B**; 2.71 g, 14.9 mmol) in EtOH (70.0 mL), then stirred for 20 h, resulting in the precipitation of **AB** as a white solid. The mixture was filtered and the precipitate was washed with EtOH and dried in vacuo (3.65 g, 83 %): M.p. 180-183 °C. Anal. Found: C 54.22; H 6.20; N 31.46. Calc. for $C_{14}H_{19}N_7O \cdot \frac{1}{2}H_2O$: C 54.18; H 6.50; N 31.59. 1H NMR (500 MHz, $CDCl_3$) δ /ppm: 7.87 (1H, d, $J=7.8$ Hz, H12), 7.75 (1H, s, H10), 7.68 (1H, t, $J=7.8$ Hz, H13), 7.14 (1H, d, $J=7.6$ Hz, H14), 6.80 (1H, s, H5), 4.75 (2H, s, H17), 4.17 (2H, bs, NH_2), 3.64 (3H, s, H8), 3.30 (3H, s, H9), 2.45 (3H, s, H7). ^{13}C NMR (500 MHz, $CDCl_3$) δ /ppm: 166.3 (C2), 165.4 (C6), 162.8 (C4), 158.7 (C15), 154.1 (C11), 137.2 (C13), 136.2 (C10), 119.6 (C14), 118.2 (C12), 82.0 (C5), 64.3 (C17), 40.0 (C9), 30.0 (C8), 26.4 (C7). ESMS m/z Found: 302.1705, 324.1527. Calc. for $C_{14}H_{20}N_7O^+$: 302.1724. Calc. for $C_{14}H_{19}N_7ONa^+$: 324.1543. Selected IR ν/cm^{-1} : 3332m (NH), 3167br (OH), 2936m (CH), 1621s (NH), 1588s, 1566s (C=N), 1539s, 1485s, 1476s, 1456s, 1440s, 1417s, 1392s, 1292s, 1268s, 1236s, 1217s, 1155s, 1091s, 1027s. Colourless crystals suitable for X-ray diffraction were grown by the slow evaporation of a $CDCl_3$ solution of **AB**.

2-Phenylpyrimidine-4,6-dicarboxaldehyde, bis[methyl][6-[1-methyl-2-(6-hydroxy-methylpyridin-2-ylmethylene)-hydrazino]-2-methylpyrimidin-4-yl]hydrazone (L1). **AB** (2.15 g, 7.16 mmol) and 2-phenyl-4,6-pyrimidinedicarboxaldehyde (**C**; 0.727 g, 3.42 mmol) were refluxed in EtOH (250 mL) for 6 h resulting in the precipitation of **L1** as a white solid. The mixture was filtered and the precipitate was washed with EtOH and dried in vacuo (2.31 g, 87 %): Anal. Found: C 60.19; H 5.36; N 28.40. Calc. for $C_{40}H_{42}N_{16}O_2 \cdot H_2O$: C 60.29; H 5.57; N 28.12. 1H NMR (500 MHz, $CDCl_3$) δ /ppm: 8.52 (2H, m, H8), 8.49 (1H, s, H5), 7.78 (2H, s, H11), 7.64 (2H, d, $J=7.7$ Hz, H21), 7.53 (3H, m, H9/H10), 7.44 (2H, s, H19), 7.31 (2H, s, H14), 7.11 (2H, t, $J=7.6$ Hz, H22), 6.81 (2H, d, $J=7.5$ Hz, H23), 4.61 (4H, s, H25), 3.92 (2H, bs, H26), 3.57 (6H, s, H12), 3.49 (6H, s, H18), 2.46 (6H, s, H17). ^{13}C NMR (500 MHz, $CDCl_3$) δ /ppm: 165.7 (C16), 165.2 (C2), 162.5 (C15), 162.4 (C4, C6), 162.0 (C13), 158.5 (C24), 153.5 (C20), 136.4 (C7), 136.4 (C19), 134.9 (C11), 130.9 (C10), 128.8 (C9), 128.3 (C8), 119.2 (C23), 118.1 (C21), 107.1 (C5), 87.4 (C14), 64.7 (C25), 30.1 (C12), 29.7 (C18), 26.0 (C17). ESMS m/z Found: 779.3739, 801.3561. Calc. for $C_{40}H_{43}N_{16}O_2^+$: 779.89; Calc. for $C_{40}H_{42}N_{16}O_2Na^+$: 801.3569. Selected IR ν/cm^{-1} : 3373br (OH), 2919w (CH), 1589s, 1559s (C=N), 1528m, 1482s, 1455m, 1432m, 1409m, 1386m, 1369m, 1280w, 1264w, 1236m, 1215m, 1165m, 1093w, 1042m. Colourless crystals suitable for X-ray diffraction were grown by slow diffusion of diethyl ether into a CH_2Cl_2 solution of **L1**.

2-Phenylpyrimidine-4,6-dicarboxaldehyde, bis[methyl][6-[1-methyl-2-(6-hydroxy-methylacryloylpyridin-2-ylmethylene)hydrazino]-2-methylpyrimidin-4-yl]hydrazine (L2). Acryloyl chloride (1.00 mL, 12.3 mmol) was added dropwise to a mixture of **L1** (1.04 g, 1.33 mmol) and triethylamine (2.00 mL, 14.4 mmol) stirring in dry CH_2Cl_2 (250 mL) under Ar. The resulting orange solution was then stirred at 60 °C for 4 h under Ar, then cooled to rt and added to H_2O (50.0 mL). The organic layer was separated and washed with H_2O , saturated NaCl

solution and Na₂CO₃ solution before being dried over MgSO₄. It was then rotary evaporated to dryness and the resulting brown solid residue was stirred in acetone (10.0 mL) for 1 h, resulting in the precipitation of **L2** as a white solid (0.839 g, 71 %): Anal. Found: C 61.71; H 5.24; N 23.30. Calc. for C₄₆H₄₆N₁₆O₂·½H₂O: C 61.66; H 5.29; N 25.01. ¹H NMR (500 MHz, CDCl₃) δ/ppm: 8.55 (2H, m, H8), 8.52 (1H, s, H5), 7.85 (2H, s, H11), 7.72 (2H, d, J=7.8 Hz, H21), 7.54 (3H, m, H9/10), 7.52 (2H, s, H19), 7.30 (2H, s, H14), 7.12 (2H, t, J=7.7 Hz, H22), 6.90 (2H, d, J=7.5 Hz, H23), 6.54 (2H, dd, J=1.3, 17.3 Hz, H28a), 6.26 (2H, dd, J=10.5, 17.3 Hz, H27), 5.92 (2H, dd, J=1.3, 10.5 Hz, H28b), 5.21 (4H, s, H25), 3.65 (6H, s, H12), 3.49 (6H, s, H18), 2.42 (6H, s, H17). ¹³C NMR (500 MHz, CDCl₃) δ/ppm: 166.0 (C26), 165.6 (C16), 165.2 (C2), 162.5 (C16), 162.4 (C4/6), 162.2 (C13), 154.9 (C24), 154.1 (C20), 137.9 (C7), 136.7 (C22), 136.4 (C19), 135.3 (C11), 131.8 (C28), 131.0 (C10), 128.9 (C9), 128.4 (C8), 128.3 (C27), 120.0 (C23), 118.6 (C21), 107.1 (C5), 87.2 (C14), 66.8 (C25), 30.3 (C12), 29.9 (C18), 26.2 (C17). ESMS *m/z* Found: 909.3705. Calc. for C₄₆H₄₆N₁₆O₄Na⁺: 909.3786. Selected IR ν/cm⁻¹: 2920m (CH), 1728s (C=O), 1633m (C=C), 1589s, 1561s (C=N), 1525s, 1482s, 1429s, 1410s, 1369s, 1292s, 1238s, 1215s, 1166s, 1092s, 1044s.

Pb₄L1(ClO₄)₈. A solution of Pb(ClO₄)₂·3H₂O (23.2 mg, 0.0504 mmol) in CH₃CN (5.00 mL) was added to **L1** (9.65 mg, 0.0124 mmol) and stirred at 70 °C for 1 h resulting in the dissolution of **L1** and the formation of an orange solution. The addition of diethyl ether (20.0 mL) resulted in the precipitation of an orange solid, which was filtered, washed with diethyl ether and dried in vacuo (15.5 mg, 52 %): Anal. Found: C 19.54; H 2.32; N 9.00. Calc. for C₄₀H₄₂N₁₆O₃₄Cl₈Pb₄·4H₂O: C 19.41; H 2.04; N 9.05. ¹H NMR (500 MHz, CD₃CN) δ/ppm: 8.89 (2H, s, H11), 8.79 (2H, s, H19), 8.38 (1H, s, H5), 8.20 (2H, t, J=7.8 Hz, H22), 7.97 (2H, d, J=7.5 Hz, H21), 7.97 (2H, m, H8), 7.85 (3H, m, H9/10), 7.69 (2H, d, J=7.9 Hz, H23), 6.83 (2H, s, H14), 6.12 (2H, br, H26), 5.33 (4H, s, H25), 3.85 (6H, s, H12), 3.78 (6H, s, H18), 2.79 (6H, s, H17). ¹³C NMR (500 MHz, CD₃CN) δ/ppm: 168.0 (C2), 167.4 (C16), 162.0 (C24), 161.0 (C15), 160.2 (C4/6), 160.0 (C13), 149.7 (C20), 145.7 (C19), 142.3 (C11), 141.7 (C22), 136.4 (C7), 133.1 (C9), 132.3 (C8), 128.6 (C10), 128.3 (C21), 125.2 (C23), 124.1 (C5), 88.7 (C14), 65.2 (C25), 36.5 (C12), 35.8 (C18), 26.5 (C17). ESMS *m/z* Found: 1491.1700, 596.1525. Calc. for C₄₀H₄₂N₁₆O₂Pb₂·(ClO₄)₃⁺: 1491.1665. Calc. for C₄₀H₄₀N₁₆O₂Pb₂²⁺: 596.1521. Selected IR ν/cm⁻¹: 3445br (OH), 3070w (CH), 2924w (CH), 1636w, 1588m, 1545s (C=N), 1475m, 1448m, 1412m, 1381m, 1292m, 1267m, 1152s, 1110s, 1089s, 1047s (ClO₄). Crystals suitable for X-ray diffraction were grown by the slow diffusion of diethyl ether into a CH₃NO₂ solution of Pb(ClO₄)₂·3H₂O and **L1** in a 4:1 metal to ligand ratio. These crystals gave the structure [Pb₄L1(ClO₄)₇(H₂O)]ClO₄·4CH₃NO₂ (**1**).

Pb₄L1(SO₃CF₃)₈. As described for Pb₄L1(ClO₄)₈ but with Pb(SO₃CF₃)₂·H₂O (112 mg, 0.220 mmol) and **L1** (41.8 mg, 0.0537 mmol) in CH₃CN (5.00 mL); orange solid (117 mg, 78 %): Anal. Found: C 19.65; H 1.99; N 7.38. Calc. for C₄₈H₄₂N₁₆O₂₆F₂₄S₈Pb₄·8H₂O: C 19.58; H 1.99; N 7.61. ¹H NMR (500 MHz, CD₃CN) δ/ppm: 8.94 (2H, br, H11), 8.76 (2H, s, H19), 8.44 (1H, br, H5), 8.23 (2H, t, J=7.8 Hz, H22), 8.11 (2H, br, H8), 7.96 (2H, d, J=7.5 Hz, H21), 7.84 (3H, br, H9/10), 7.71 (2H, d, J=7.9 Hz, H23), 6.86 (2H, br, H14), 5.35 (4H, s, H25), 3.86 (6H, s, H12), 3.80 (6H, s, H18), 2.82 (6H, s, H17). ¹³C NMR (500 MHz, CD₃CN) δ/ppm: 168.4 (br, C4/C6), 198.0 (C16), 162.7 (C24), 161.5 (C15), 160.6 (C13), 150.5 (C20), 145.7 (C19), 142.2 (C22), 133.4 (C7), 132.3 (C8), 129.4

(C2), 128.5 (C21), 125.4 (C23), 88.6 (C14), 65.6 (C25), 36.9 (C12), 36.3 (C18), 26.4 (C17). ESMS *m/z* Found: 801.3553. Calc. for C₄₀H₄₂N₁₆O₂Na⁺: 801.3569. Selected IR ν/cm⁻¹: 3379br (OH), 1588m, 1542s (C=N), 1476m, 1448m, 1383m, 1358m, 1211s (SO₃CF₃), 1149s, 1049s, 1017s. Crystals suitable for X-ray were grown by the slow diffusion of diethyl ether into a CH₃CN solution of Pb(SO₃CF₃)₂·H₂O and **L1** in a 4:1 metal to ligand ratio. These crystals gave the structure [Pb₄L1(SO₃CF₃)₈]₂·6CH₃CN·H₂O (**2**).

Pb₂L1(ClO₄)₄. As described for Pb₄L1(ClO₄)₈ but with Pb(ClO₄)₂·3H₂O (94.4 mg, 0.205 mmol) and **L1** (79.3 mg, 0.102 mmol) in CH₃CN (10.0 mL); yellow solid (98.7 mg, 61 %): Anal. Found: C 30.06; H 3.09; N 13.83. Calc. for C₄₀H₄₂N₁₆O₁₈Cl₄Pb₂·H₂O: C 29.86; H 2.76; N 13.93. ¹H NMR (500 MHz, CD₃CN/(CD₃)₂CO) δ/ppm: 8.48 (2H, s, H19), 8.44 (2H, m, H8), 8.33 (1H, s, H5), 7.95 (2H, s, H11), 7.80 (2H, t, J=7.7 Hz, H22), 7.53 (2H, d, J=7.7 Hz, H23), 7.50 (2H, m, H21), 7.47 (3H, m, H9/10), 7.27 (2H, s, H14), 6.49 (2H, s, H26), 5.34 (4H, s, H25), 3.71 (6H, s, H12), 3.60 (6H, s, H18), 2.74 (6H, s, H17). ESMS *m/z* Found: 801.3659. Calc. for C₄₀H₄₂N₁₆O₂Na⁺: 801.3569. Selected IR ν/cm⁻¹: 3389br (OH), 2921w (CH), 1576m, 1551s (C=N), 1478m, 1447m, 1407m, 1369m, 1315m, 1285m, 1230m, 1194m, 1090s, 1042s (ClO₄). Crystals suitable for X-ray diffraction were grown by the slow diffusion of diethyl ether into a CH₃CN solution of Pb(ClO₄)₂·3H₂O and **L1** in a 2:1 metal to ligand ratio. These crystals gave the structure [Pb₂L1(ClO₄)₂(CH₃CN)(H₂O)]·(ClO₄)₂·2CH₃CN·C₄H₁₀O·H₂O (**3**).

Pb₂L1(SO₃CF₃)₄. As described for Pb₄L1(ClO₄)₈ but with Pb(SO₃CF₃)₂·H₂O (46.6 mg, 0.089 mmol) and **L1** (32.2 mg, 0.042 mmol) in CH₃CN (10.0 mL); yellow solid (45.3 mg, 60 %): Anal. Found: C 28.36; H 2.54; N 11.81. Calc. for C₄₄H₄₂N₁₆O₁₄F₁₂S₄Pb₂·4H₂O: C 28.39; H 2.71; N 12.04. ¹H NMR (500 MHz, CD₃CN/(CD₃)₂CO) δ/ppm: 8.48 (2H, m, H8), 8.42 (2H, s, H19), 8.38 (1H, s, H5), 8.00 (2H, s, H11), 7.71 (2H, t, J=7.7 Hz, H22), 7.50 (5H, m, H9/10/21), 7.43 (2H, d, J=7.5 Hz, H23), 7.28 (2H, s, H14), 6.05 (2H, t, J=3.5 Hz, H26), 5.30 (4H, d, J=3.6 Hz, H25), 3.74 (6H, s, H12), 3.57 (6H, s, H18), 2.75 (6H, s, H17). ESMS *m/z* Found: 801.3528. Calc. for C₄₀H₄₂N₁₆O₂Na⁺: 801.3569. Selected IR ν/cm⁻¹: 3356br (OH), 3097w (CH), 2963w (CH), 2928w (CH), 1726w, 1682w, 1589m, 1577m, 1548s (C=N), 1479m, 1445m, 1411m, 1371m, 1279s, 1208s (SO₃CF₃), 1163s, 1117s, 1047s, 1017s.

Pb₄L2(ClO₄)₈. As described for Pb₄L1(ClO₄)₈ but with Pb(ClO₄)₂·3H₂O (135 mg, 0.289 mmol) and **L2** (61.4 mg, 0.0692 mmol) in CH₃CN (10.0 mL); orange solid (136 mg, 78 %): Anal. Found: C 21.17; H 2.25; N 8.34. Calc. for C₄₆H₄₆N₁₆O₃₆Pb₄Cl₈·4H₂O: C 21.39; H 2.11; N 8.67. ¹H NMR (500 MHz, CD₃CN) δ/ppm: 8.96 (2H, s, H19), 8.94 (2H, s, H11), 8.28 (1H, s, H5), 8.26 (2H, t, J=7.8 Hz, H22), 8.07 (2H, d, J=7.7 Hz, H21), 7.97 (2H, d, J=3.6 Hz, H8), 7.86 (2H, d, J=7.9 Hz, H23), 7.86 (3H, m, H9/10), 6.90 (2H, s, H14), 6.46 (2H, dd, J=1.0, 17.3 Hz, H28a), 6.29 (2H, dd, J=10.5, 17.3 Hz, H27), 5.99 (2H, dd, J=1.0, 10.5 Hz, H28b), 5.48 (4H, s, H25), 3.86 (6H, s, H12), 3.80 (6H, s, H18), 2.83 (6H, s, H17). ¹³C NMR (500 MHz, CD₃CN) δ/ppm: 167.9 (C2), 167.3 (C16), 166.3 (C26), 160.3 (C13/15), 160.0 (C11), 156.8 (C24), 149.4 (C20), 147.5 (C19), 142.9 (C4/6), 142.5 (C22), 136.4 (C7), 133.8 (C28), 133.1 (C9), 132.3 (C10), 129.6 (C21), 128.5 (C8), 128.2 (C23), 127.8 (C27), 124.3 (C5), 88.8 (C14), 65.9 (C25), 36.6 (C12), 35.9 (C18), 26.1 (C17). ESMS *m/z* Found: 909.3699, 887.3966. Calc. for C₄₆H₄₆N₁₆O₄Na⁺: 909.3785. Calc. for C₄₆H₄₇N₁₆O₄⁺: 887.3966. Selected IR ν/cm⁻¹: 3406w, 3064w (CH), 1707w (C=O), 1587m, 1543s (C=N), 1478m,

1460m, 1449m, 1408m, 1384m, 1295m, 1264m, 1153m, 1043s (ClO₄⁻).

Pb₄L2(SO₃CF₃)₈. As described for Pb₄L1(ClO₄)₈ but with Pb(SO₃CF₃)₂·H₂O (135 mg, 0.258 mmol) and **L2** (56.6 mg, 0.0638 mmol) in CH₃CN (10.0 mL); orange solid (116 mg, 62 %): Anal. Found: C 22.39; H 1.98; N 7.48. Calc. for C₅₄H₄₆N₁₆O₂₈Pb₄S₈F₂₄·H₂O: C 22.16; H 1.65; N 7.66. ¹H NMR (500 MHz, CD₃CN) δ/ppm: 8.94 (4H, s, H11/H19), 8.43 (1H, s, H5), 8.29 (2H, t, J=7.8 Hz, H22), 8.07 (2H, d, J=7.9 Hz, H21), 8.07 (2H, m, H8), 7.88 (2H, d, J=7.7 Hz, H23), 7.88 (3H, m, H9/10), 6.94 (2H, s, H14), 6.51 (2H, d, J=17.3 Hz, H28a), 6.34 (2H, dd, J=10.4, 17.3 Hz, H27), 6.00 (2H, d, J=10.6 Hz, H28b), 5.54 (4H, s, H25), 3.88 (6H, s, H12), 3.81 (6H, s, H18), 2.83 (6H, s, H17). ESMS *m/z* Found: 909.3785. Calc. for C₄₆H₄₆N₁₆O₄Na⁺: 909.3781. Selected IR ν/cm⁻¹: 3356w, 3066w (CH), 1710w (C=O), 1590m, 1576m, 1545s (C=N), 1481m, 1461m, 1411m, 1389m, 1212s (SO₃CF₃⁻), 1149s, 1049s, 1016s.

Pb₂L2(ClO₄)₄. As described for Pb₄L1(ClO₄)₈ but with Pb(ClO₄)₂·3H₂O (25.6 mg, 0.0556 mmol) and **L2** (23.3 mg, 0.0263 mmol) in CH₃CN (10.0 mL); yellow solid (32.8 mg, 74 %): Anal. Found: C 31.19; H 2.82; N 12.45. Calc. for C₄₆H₄₆N₁₆O₂₆Cl₄Pb₂·4H₂O: C 31.19; H 3.07; N 12.65. ¹H NMR (500 MHz, CD₃CN/(CD₃)₂CO) δ/ppm: 8.61 (2H, s, H19), 8.54 (3H, m, H5/8), 8.12 (2H, s, H11), 7.84 (2H, t, J=7.9 Hz, H22), 7.72 (2H, d, J=7.7 Hz, H21), 7.55 (5H, m, H9/10/23), 7.47 (2H, s, H14), 6.57 (2H, d, J=17.2 Hz, H28a), 6.43 (2H, dd, J=10.3, 17.3 Hz, H27), 6.05 (2H, d, J=10.3 Hz, H28b), 5.54 (4H, s, H25), 3.84 (6H, s, H12), 3.64 (6H, s, H18), 2.81 (6H, s, H17). ESMS *m/z* Found: 909.3750. Calc. for C₄₆H₄₆N₁₆O₄Na⁺: 909.3781. Selected IR ν/cm⁻¹: 3447br, 3085w (CH), 3050w (CH), 1713w (C=O), 1630w (C=C), 1590m, 1576m, 1552s (C=N), 1479m, 1459m, 1459m, 1408m, 1392m, 1371m, 1315m, 1289s, 1230s, 1093s, 1046s (ClO₄⁻).

Pb₂L2(SO₃CF₃)₄. As described for Pb₄L1(ClO₄)₈ but with Pb(SO₃CF₃)₂·H₂O (34.8 mg, 0.0665 mmol) and **L2** (27.5 mg, 0.0310 mmol) in CH₃CN (10.0 mL); yellow solid (38.1 mg, 65 %): Anal. Found: C 31.98; H 2.64; N 11.48. Calc. for C₅₀H₄₆N₁₆O₁₆F₁₂S₄Pb₂: C 31.65; H 2.44; N 11.81. ¹H NMR (500 MHz, CD₃CN/(CD₃)₂CO) δ/ppm: 8.57 (2H, s, H19), 8.51 (2H, m, H8), 8.48 (1H, s, H5), 8.06 (2H, s, H11), 7.69 (4H, m, H21/22), 7.53 (3H, m, H9/10), 7.46 (2H, d, J=7.1 Hz, H23), 7.38 (2H, s, H14), 6.58 (2H, dd, J=1.3, 17.3 Hz, H28a), 6.42 (2H, dd, J=10.3, 17.3 Hz, H27), 6.05 (2H, dd, J=1.4, 10.4 Hz, H28b), 5.52 (4H, s, H25), 3.78 (6H, s, H12), 3.59 (6H, s, H18), 2.80 (6H, s, H17). ESMS *m/z* Found: 909.3760. Calc. for C₄₆H₄₆N₁₆O₄Na⁺: 909.3781. Selected IR ν/cm⁻¹: 3404w, 3075w (CH), 3045w (CH), 1719w (C=O), 1631w (C=C), 1590m, 1577m, 1552s (C=N), 1480m, 1458m, 1408m, 1458m, 1408m, 1371m, 1281m, 1225s (SO₃CF₃⁻), 1207s, 1160s, 1117s, 1048s, 1015s.

Zn₄L1(SO₃CF₃)₈. As described for Pb₄L1(ClO₄)₈ but with Zn(SO₃CF₃)₂ (310 mg, 0.852 mmol) and **L1** (64.7 mg, 0.0831 mmol) in CH₃CN (5.00 mL); orange solid (126 mg, 68 %): Anal. Found: C 25.00; H 2.57; N 9.33. Calc. for C₄₈H₄₂N₁₆O₂₆F₂₄S₈Zn₄·6H₂O: C 24.63; H 2.33; N 9.57. ¹H NMR (500 MHz, CD₃CN) δ/ppm: 8.53 (2H, s, H11), 8.38 (2H, s, H19), 8.36 (1H, s, H5), 8.19 (2H, t, J=7.8 Hz, H22), 7.86 (2H, d, J=7.1 Hz, H8), 7.85 (2H, d, J=7.9 Hz, H21), 7.80 (1H, d, J=7.4 Hz, H10), 7.76 (2H, t, J=7.4 Hz, H9), 7.63 (2H, d, J=8.0 Hz, H23), 6.90 (2H, s, H14), 6.81 (2H, t, J=3.5 Hz, H26), 5.05 (4H, d, J=3.5 Hz, H25), 3.88 (6H, s, H12), 3.79 (6H, s, H18), 2.81 (6H, s, H17). ¹³C NMR (500 MHz, CD₃CN) δ/ppm: 168.9 (C2), 167.8 (C16), 159.5 (C11), 159.4 (C15), 158.6 (C4/6), 158.3 (C24), 146.1 (C20), 143.3 (C22), 137.0 (C19),

136.2 (C7), 135.0 (C11), 133.1 (C10), 131.0 (C8), 129.9 (C9), 126.0 (C21), 125.1 (C23), 123.4 (C5), 88.3 (C14), 61.7 (C25), 35.8 (C12), 34.5 (C18), 27.5 (C17). ESMS *m/z* Found: 1357.0799, 603.0645. Calc. for C₄₀H₄₂N₁₆O₂Zn₂(SO₃CF₃)₃⁺: 1355.0784. Calc. for C₄₀H₄₂N₁₆O₂Zn₂(SO₃CF₃)₂²⁺: 603.0629. Selected IR ν/cm⁻¹: 3294br (OH), 1559s (C=N), 1479m, 1447m, 1383m, 1282m, 1232s (SO₃CF₃⁻), 1212s, 1149s, 1055s, 1022s.

Zn₄L2(SO₃CF₃)₈. As described for Pb₄L1(ClO₄)₈ but with Zn(SO₃CF₃)₂ (279 mg, 0.768 mmol) and **L2** (54.8 mg, 0.0619 mmol) in CH₃CN (5.00 mL); orange solid (110 mg, 79 %): Anal. Found: C 26.83; H 2.85; N 9.08. Calc. for C₅₄H₄₆N₁₆O₂₈Zn₄S₈F₂₄·CH₃CN·8H₂O: C 26.63; H 2.59; N 9.43. ¹H NMR (500 MHz, CD₃CN) δ/ppm: 8.52 (2H, s, H11), 8.47 (2H, s, H19), 8.38 (1H, s, H5), 8.22 (2H, t, J=7.8 Hz, H22), 7.91 (2H, d, J=7.6 Hz, H21), 7.84 (4H, d, J=7.8 Hz, H8/H23), 7.76 (1H, t, J=7.3 Hz, H10), 7.70 (2H, m, H9), 6.92 (2H, s, H14), 6.47 (2H, d, J=17.4 Hz, H28a), 6.25 (2H, dd, J=10.5, 17.3 Hz, H27), 5.99 (2H, d, J=10.6 Hz, H28b), 5.50 (4H, s, H25), 3.84 (6H, s, H12), 3.76 (6H, s, H18), 2.81 (6H, s, H17). ¹³C NMR (500 MHz, CD₃CN) δ/ppm: 169.2 (C16), 169.1 (C2), 168.0 (C26), 159.8 (C13), 159.3 (C15), 158.8 (C4/6), 158.4 (C24), 147.6 (C20), 144.0 (C22), 139.7 (C19), 136.2 (C7), 135.5 (C11), 134.4 (C28), 133.4 (C10), 131.2 (C9), 130.0 (C8), 128.5 (C21), 128.5 (C27), 128.0 (C23), 123.5 (C5), 88.4 (C14), 66.3 (C25), 36.0 (C12), 35.0 (C18), 26.9 (C17). ESMS *m/z* Found: 909.3766. Calc. for C₄₆H₄₆N₁₆O₄Na⁺: 909.3781. Selected IR ν/cm⁻¹: 3248br, 1730w (C=O), 1659w (C=C), 1601m, 1579m, 1556s (C=N), 1481m, 1410m, 1372m, 1282s, 1223s (SO₃CF₃⁻), 1160s, 1116s, 1052s, 1024s.

Cu₄L1(ClO₄)₈. As described for Pb₄L1(ClO₄)₈ but with Cu(ClO₄)₂·6H₂O (61.1 mg, 0.165 mmol) and **L1** (31.8 mg, 0.0409 mmol) in CH₃CN (10.0 mL); green solid (65.4 mg, 87 %): Anal. Found: C 27.37; H 2.96; N 12.58. Calc. for C₄₀H₄₂N₁₆O₃₄Cl₈Cu₄·2CH₃CN·2H₂O: C 27.15; H 2.69; N 12.95. ESMS *m/z* Found: 940.2481, 451.1048. Calc. for C₄₀H₄₂N₁₆O₂Cu₄(ClO₄)₄⁺: 940.2478. Calc. for C₄₀H₄₀N₁₆O₂Cu₂²⁺: 451.1051. Selected IR ν/cm⁻¹: 3452br (OH), 3067w (CH), 2939w (CH), 1627m, 1601m, 1556s (C=N), 1476m, 1432m, 1381m, 1289m, 1152m, 1048s (ClO₄⁻). UV-Vis λ_{max}(ε)/nm(L mol⁻¹ cm⁻¹): 690 (449).

Cu₄L1(SO₃CF₃)₈. As described for Pb₄L1(ClO₄)₈ but with Cu(SO₃CF₃)₂ (68.1 mg, 0.157 mmol) and **L1** (30.4 mg, 0.0391 mmol) in CH₃CN (10.0 mL); green solid (71.2 mg, 81 %): Anal. Found: C 25.47; H 2.15; N 9.86. Calc. for C₄₈H₄₂N₁₆O₂₆F₂₄S₈Cu₄·2H₂O: C 25.49; H 2.05; N 9.91. ESMS *m/z* Found: 801.3587. Calc. for C₄₀H₄₂N₁₆O₂Na⁺: 801.3569. Selected IR ν/cm⁻¹: 3357br (OH), 3067w (CH), 1603m, 1557s (C=N), 1482m, 1383m, 1220s (SO₃CF₃⁻), 1148s, 1057s, 1022s. UV-Vis λ_{max}(ε)/nm(L mol⁻¹ cm⁻¹): 691 (417).

Cu₄L2(ClO₄)₈. As described for Pb₄L1(ClO₄)₈ but with Cu(ClO₄)₂·6H₂O (85.3 mg, 0.231 mmol) and **L2** (47.1 mg, 0.0531 mmol) in CH₃CN (10.0 mL); green solid (80.4 mg, 78 %): Anal. Found: C 24.58; H 3.26; N 10.32. Calc. for C₄₆H₄₆N₁₆O₃₆Cl₈Cu₄·16H₂O: C 24.83; H 3.53; N 10.07. ESMS *m/z* Found: 909.3788. Calc. for C₄₆H₄₆N₁₆O₄Na⁺: 909.3781. Selected IR ν/cm⁻¹: 3425m, 3064w (CH), 1720w (C=O), 1656w (C=C), 1631w, 1587m, 1552s (C=N), 1472m, 1435m, 1415m, 1383m, 1292m (CO), 1266m, 1155m, 1052s (ClO₄⁻). UV-Vis λ_{max}(ε)/nm(L mol⁻¹ cm⁻¹): 687 (508).

Cu₄L2(SO₃CF₃)₈. As described for Pb₄L1(ClO₄)₈ but with Cu(SO₃CF₃)₂·4H₂O (101 mg, 0.235 mmol) and **L2** (49.9 mg, 0.0563 mmol) in CH₃CN (10.0 mL); green solid (96.7 mg, 74 %): Anal. Found: C 26.44; H 2.54; N 9.00. Calc. for C₅₄H₄₆N₁₆O₂₈F₂₄S₈Cu₄·8H₂O: C 26.18; H 2.52; N 9.04. ESMS

m/z Found: 909.3699. Calc. for $C_{46}H_{46}N_{16}O_4Na^+$: 909.3781. Selected IR ν/cm^{-1} : 3245w, 3118w (CH), 3064w (CH), 1719w (C=O), 1656w (C=C), 1628w, 1604w, 1577m, 1551s (C=N), 1481m, 1416m, 1383w, 1282s (CO), 1221s ($SO_3CF_3^-$), 1149s, 1057s, 1023s. UV-Vis λ_{max} (ϵ)/nm ($L\ mol^{-1}\ cm^{-1}$): 684 (546). Crystals suitable for X-ray were grown by the slow diffusion of diethyl ether into a CH_3CN solution of $Cu(SO_3CF_3)_2 \cdot 4H_2O$ and **L2** in a 4:1 metal to ligand ratio. These crystals gave the structure $[Cu_3L_2(SO_3CF_3)_3(CH_3CN)_2(H_2O)](SO_3CF_3)_3 \cdot 2CH_3CN \cdot H_2O$ (**4**).

Ag₂L₁(SO₃CF₃)₂. As described for $Pb_4L_1(ClO_4)_8$ but with $AgSO_3CF_3$ (11.7 mg, 0.0457 mmol) and **L1** (31.0 mg, 0.0398 mmol) in CH_3CN (5.00 mL); yellow solid (30.6 mg): Anal. Found: C 45.39; H 4.06; N 20.41. Calc. for $C_{41}H_{42}N_{16}O_5F_3SAg^{1/2}AgSO_3CF_3$: C 45.52; H 3.89; N 20.61. 1H NMR (500 MHz, CD_3CN) δ/ppm : 8.54 (2H, m, H8), 7.87 (2H, t, J=7.7 Hz, H22), 7.68 (1H, s, H5), 7.66 (3H, m, H9/10), 7.46 (2H, s, H19), 7.29 (2H, d, J=7.7 Hz, H21), 7.22 (2H, d, J=7.8 Hz, H23), 6.97 (2H, s, H11), 6.83 (2H, s, H14), 3.79 (4H, d, J=5.5 Hz, H25), 3.36 (2H, t, J=5.6 Hz, H26), 3.12 (6H, s, H18), 2.93 (6H, s, H12), 2.19 (6H, s, H17). ESMS *m/z* Found: 1921.5064, 1141.1256, 885.2805. Calc. for $(C_{40}H_{42}N_{16}O_2)_2-Ag_2(SO_3CF_3)^+$: 1919.4975. Calc. for $C_{40}H_{42}N_{16}O_2Ag_2(SO_3CF_3)^+$: 1141.1299. Calc. for $C_{40}H_{42}N_{16}O_2Ag^+$: 885.2728. Selected IR ν/cm^{-1} : 3387br (OH), 3066w (CH), 3015w (CH), 2916w (CH), 2872w (CH), 1707w, 1572m, 1541s (C=N), 1527s, 1475s, 1458m, 1426m, 1406s, 1388m, 1365s, 1312w, 1272m (CO), 1246s, 1235s, 1222s ($SO_3CF_3^-$), 1153s, 1087m, 1041s, 1026s. Crystals suitable for X-ray were grown by the slow diffusion of diethyl ether into a CH_3CN solution of $AgSO_3CF_3$ and **L1** in a 1:1 metal to ligand ratio. These crystals gave the structure $[Ag_2L_1](SO_3CF_3)_2 \cdot CH_3CN \cdot H_2O$ (**5**).

Ag₂L₁(BF₄)₂. As described for $Pb_4L_1(ClO_4)_8$ but with $AgSO_3CF_3$ (9.80 mg, 0.0505 mmol) and **L1** (29.1 mg, 0.0374 mmol) in CH_3CN (10.0 mL); yellow solid (33.1 mg): Anal. Found: C 45.42; H 3.83; N 20.94. Calc. for $C_{40}H_{42}N_{16}O_2BF_4Ag^{4/9}AgBF_4$: C 45.32; H 3.99; N 21.14. 1H NMR (500 MHz, CD_3NO_2) δ/ppm : 8.52 (2H, m, H8), 7.98 (2H, t, J=7.8 Hz, H22), 7.84 (1H, s, H5), 7.67 (3H, m, H9/10), 7.56 (2H, s, H19), 7.41 (2H, d, J=7.6 Hz, H21), 7.34 (2H, d, J=7.7 Hz, H23), 7.13 (2H, s, H11), 7.00 (2H, s, H14), 3.96 (4H, s, H25), 3.26 (6H, s, H18), 3.08 (6H, s, H12), 2.23 (6H, s, H17). ESMS *m/z* Found: 887.2741. Calc. for $C_{40}H_{42}N_{16}O_2Ag^+$: 885.2728. Selected IR ν/cm^{-1} : 3505br (OH), 2915w (CH), 2852w (CH), 1589w, 1569m, 1541s (C=N), 1475m, 1458m, 1426m, 1405m, 1369m, 1311m, 1277m (CO), 1234m, 1155m, 1086m, 1039s (BF_4^-).

Ag₂L₂(SO₃CF₃)₂. As described for $Pb_4L_1(ClO_4)_8$ but with $AgSO_3CF_3$ (12.7 mg, 0.0496 mmol) and **L2** (41.2 mg, 0.0465 mmol) in CH_3CN (10.0 mL); yellow solid (34.6 mg): Anal. Found: C 43.50; H 3.64; N 17.00. Calc. for $C_{47}H_{46}N_{16}O_7F_3SAg^{2/3}AgSO_3CF_3$: C 43.53; H 3.53; N 17.04. 1H NMR (500 MHz, CD_3CN) δ/ppm : 8.53 (2H, m, H8), 7.93 (2H, t, J=7.8 Hz, H22), 7.69 (1H, s, H5), 7.51 (2H, s, H19), 7.41 (2H, d, J=7.8 Hz, H21), 7.26 (2H, d, J=7.8 Hz, H23), 6.99 (2H, s, H11), 6.86 (2H, s, H14), 6.05 (2H, dd, J=1.3, 17.9 Hz, H28a), 5.78 (2H, dd, J=10.4, 17.3 Hz, H27), 5.56 (2H, dd, J=1.3, 10.4 Hz, H28b), 4.35 (2H, d, J=14.0 Hz, H25a), 4.30 (2H, d, J=14.0 Hz, H25b), 3.09 (6H, s, H18), 2.92 (6H, s, H12), 2.22 (6H, s, H17). ESMS (CH_3CN) *m/z* Found: 993.3015. Calc. for $C_{46}H_{46}N_{16}O_4Ag^+$: 993.2939. Selected IR ν/cm^{-1} : 3033w (CH), 2925w (CH), 1727m (C=O), 1633w (C=C), 1574m, 1540s (C=N), 1474m, 1456m, 1429m, 1401s, 1366s, 1253s (CO), 1222s ($SO_3CF_3^-$), 1149s, 1118s, 1090s, 1041s, 1026s.

Ag₂L₂(BF₄)₂. As described for $Pb_4L_1(ClO_4)_8$ but with $AgBF_4$ (9.31 mg, 0.0479 mmol) and **L2** (41.6 mg, 0.0470 mmol) in CH_3CN (10.0 mL); yellow solid (33.5 mg): Anal. Found: C 46.67; H 3.98; N 18.99. Calc. for $C_{46}H_{46}N_{16}O_4BF_4Ag^{1/2}AgBF_4$: C 46.86; H 3.93; N 19.01. 1H NMR (500 MHz, CD_3CN) δ/ppm : 8.52 (2H, m, H8), 7.93 (2H, t, J=7.8 Hz, H22), 7.69 (1H, s, H5), 7.66 (3H, m, H9/10), 7.51 (2H, s, H19), 7.41 (2H, d, J=7.7 Hz, H21), 7.26 (2H, d, J=7.7 Hz, H23), 6.99 (2H, s, H11), 6.86 (2H, s, H14), 6.05 (2H, dd, J=1.3, 17.3 Hz, H28a), 5.78 (2H, dd, J=10.4, 17.3 Hz, H27), 5.56 (2H, dd, J=1.3, 10.4 Hz, H28b), 4.35 (2H, d, J=14.0 Hz, H25a), 4.30 (2H, d, J=13.9 Hz, H25b), 3.09 (6H, s, H18), 2.92 (6H, s, H12), 2.22 (6H, s, H17). ESMS (CH_3CN) *m/z* Found: 993.2965. Calc. for $C_{46}H_{46}N_{16}O_4Ag^+$: 993.2939. Selected IR ν/cm^{-1} : 3034w (CH), 2922w (CH), 1724m (C=O), 1633w (C=C), 1575m, 1539s (C=N), 1474m, 1455m, 1402s, 1365s, 1278m (CO), 1260m, 1223m, 1153m, 1119m, 1037s (BF_4^-).

X-ray diffraction studies

The crystallography associated with **L1** and complexes **1-5** had a number of issues, including poor resolution data and low data/parameter ratios. Often this arose from the isolation of small thin crystals. For more details please refer to the annotated CIFs.

Crystallographic data are summarised in Table 1. Thermal ellipsoid pictures and selected bond lengths and angles for precursor **AB**, ligand **L1** and complexes **1-5** are available in supplementary material along with a description of how the disordered components of the complexes were treated. The X-ray diffraction data for **AB**, **L1** and complexes **1-3** and **5** were collected on a Bruker APEX II CCD diffractometer, with graphite monochromated Mo-K α ($\lambda = 0.71073\ \text{\AA}$) radiation. Intensities were corrected for Lorentz polarisation effects³⁴ and a multiscan absorption correction³⁵ was applied. The X-ray diffraction data for complex **4** was collected on an Agilent Supernova dual radiation source XRD with an Atlas detector, and a mirror monochromated Cu ($\lambda = 1.5418\ \text{\AA}$) radiation source. The structures were solved by direct methods (SHELXS³⁶ oSIR-97³⁷) and refined on F2 using all data by full-matrix least-squares procedures (SHELXL 97³⁸). All calculations were performed using the WinGX interface.³⁹ Detailed analyses of the extended structure were carried out using PLATON⁴⁰ and MERCURY⁴¹ (Version 3.1.1).

Conclusions

Tetratopic pym-hyz strands containing terminal hydroxymethyl (**L1**) and acryloyl (**L2**) arms were successfully synthesised and characterised. X-ray crystallography and NMR spectroscopy showed that the ligands were folded into 1 and $\frac{1}{2}$ helical turns in a similar fashion to the unmodified tetratopic pym-hyz strands reported in the literature. Their behaviour in the presence of metal ions has been investigated to a far more thorough degree than any previous tetratopic pym-hyz strand, as their $Pb(II)$, $Zn(II)$, $Cu(II)$, and $Ag(I)$ complexes have been studied. The addition of excess $Pb(II)$, $Zn(II)$ or $Cu(II)$ ions resulted in the uncoiling of **L1** and **L2** to form linear M_4LA_8 complexes, with an amplitude of extension comparable to that of an unmodified tetratopic pym-hyz strand. Grid formation was prevented at a 2:1 metal to ligand ratio by the coordinative nature of the hydroxymethyl arms and the bulk of the acryloyl arms. Instead, the $Pb(II)$ ions bound preferentially to the terminal pym-hyz-py pockets over the inner pym-hyz-pym sites to form horse shoe shaped Pb_2LA_4 complexes. This preferential

binding was also evident in the NMR spectra of the Pb_4LA_8 and Zn_4LA_8 complexes as the ions occupying the inner pym-hyz-pym sites appeared to have a higher lability than those in the terminal sites. Additionally, one of the Cu(II) ions bound to the inner pym-hyz-pym pockets was also lost from the $\text{Cu}_4\text{L2}(\text{SO}_3\text{CF}_3)_8$ complex during crystallisation, resulting in the formation of a twisted $\text{Cu}_3\text{L2}(\text{SO}_3\text{CF}_3)_6$ complex. Ag(I) ions would not bind to the pym N donors at any metal to ligand ratio, resulting in the formation of $\text{Ag}_2\text{L}_2\text{A}_2$ helicates.

L1 and **L2** represent the first pym-hyz strands which express a significant amplitude of extension and contain terminal functional groups which allow for them to be incorporated into larger polymer networks. The extensive investigation into their coordinative behaviour shows that the added functional groups do not prevent their uncoiling upon the addition of an excess of metal ions, however they do influence the structures formed at low metal to ligand ratios. These results demonstrate their potential for use as dynamic molecular hosts for use in novel polymer gel actuator systems.

Table 1. Crystallographic Data

	AB	L1	1	2
Formula	$\text{C}_{14}\text{H}_{19}\text{H}_7\text{O}$	$\text{C}_{40}\text{H}_{42}\text{N}_{16}\text{O}_2$	$\text{C}_{44}\text{H}_{58}\text{Cl}_8\text{N}_{20}\text{O}_{44}\text{Pb}_4$	$\text{C}_{110}\text{H}_{105}\text{F}_{48}\text{N}_{39}\text{O}_{53}\text{Pb}_8\text{S}_{16}$
Formula weight	301.36	778.90	2683.46	5904.00
Crystal system	Monoclinic	Tetragonal	Triclinic	Triclinic
Space group	$P2_1/n$	$I4_1/a$	$P-1$	$P-1$
$a/\text{\AA}$	11.7201(15)	33.8887(17)	9.2296(10)	18.0882(18)
$b/\text{\AA}$	8.1454(10)	33.8887	17.3147(18)	19.955(3)
$c/\text{\AA}$	15.683(3)	15.8396(10)	25.755(3)	26.553(3)
α°	90	90	102.491(4)	70.191(5)
β°	100.962(5)	90	96.675(4)	87.643(5)
γ°	90	90	104.479(4)	87.432(5)
$V/\text{\AA}^3$	1469.8(4)	18191.1(13)	3860.3(7)	9004.7(17)
Z	4	16	2	2
T/K	90(2)	90(2)	90(2)	90(2)
μ/mm^{-1}	0.093	0.076	9.087	7.774
Reflections collected	9733	91123	39972	93775
Unique reflections (R_{int})	2673 (0.0383)	5861 (0.0443)	8364 (0.0620)	33396 (0.0510)
R_1 indices [$I > 2\sigma(I)$]	0.0597	0.0665	0.0564	0.0706
wR2 (all data)	0.1563	0.1684	0.1389	0.1804
Goodness-of-fit	1.034	1.156	1.030	0.104
	3	4	5	
Formula	$\text{C}_{96}\text{H}_{112}\text{Cl}_8\text{N}_{38}\text{O}_{41}\text{Pb}_4$	$\text{C}_{60}\text{H}_{62}\text{Cu}_3\text{F}_{18}\text{N}_{20}\text{O}_{24}\text{S}_6$	$\text{C}_{84}\text{H}_{89}\text{Ag}_2\text{F}_6\text{N}_{35}\text{O}_{11}\text{S}_2$	
Formula weight	3566.64	2172.28	2130.77	
Crystal system	Monoclinic	Triclinic	Triclinic	
Space group	$C2/c$	$P-1$	$P-1$	
$a/\text{\AA}$	29.752(3)	11.93796(15)	15.957(3)	
$b/\text{\AA}$	10.5359(9)	18.6842(2)	16.872(3)	
$c/\text{\AA}$	44.383(4)	21.6335(2)	17.655(3)	
α°	90	113.9013(11)	90.879(8)	
β°	109.239(3)	92.2282(9)	104.340(8)	
γ°	90	105.8198(11)	99.074(8)	
$V/\text{\AA}^3$	13135(4)	4182.87(9)	4540.1(14)	
Z	4	2	2	
T/K	90(2)	100(2)	90(2)	
μ/mm^{-1}	5.368	3.413	0.569	
Reflections collected	43553	96122	22229	
Unique reflections (R_{int})	12429 (0.0559)	14909 (0.0451)	7056 (0.0557)	
R_1 indices [$I > 2\sigma(I)$]	0.0698	0.0838	0.0695	
wR2 (all data)	0.1544	0.2487	0.01691	
Goodness-of-fit	0.0698	1.042	1.065	

Acknowledgements

We thank the Department of Chemistry, University of Otago and the New Economic Research Fund of the Foundation for Research, Science and Technology (NERF Grant No UOO-X0808) for financial support.

Notes and references

- (a) J.-M. Lehn, *Angew. Chem. Int. Ed.* 2013, **52**, 2586-2850; (b) M. von Delius, D. A. Leigh, *Chem. Soc. Rev.* 2011, **40**, 3656-3676; (c) J. F. Stoddart, *Nat. Chem.* 2009, **1**, 14-15; (d) W. R. Browne, B. L. Feringa, *Nat. Nanotechnol.* 2006, **1**, 25-35.
- J. P. Abrahams, A. G. W. Leslie, R. Lutter, J. E. Walker, *Nature*, 1994, **370**, 621-648.
- (a) M. Shibata, S. Tanaka, T. Ikeda, S. Shinkai, K. Kanedo, S. Ogi, M. Takeuchi, *Angew. Chem. Int. Ed.* 2013, **52**, 397-400; (b) T. Muraoka, K. Kazushi, *J. Photochem. Photobiol. C* 2012, **13**, 136-147; (c) K. Miwa, Y. Furusho, E. Yashima, *Nat. Chem.* 2010, **2**, 444-449.
- A.-M. Stadler, N. Kyritsakas, R. Graff, J.-M. Lehn, *Chem. Eur. J.* 2006, **12**, 4503-4522.
- (a) A.-M. Stadler, J.-J. Jiang, H.-P. Wang, C. Bailly, *Chem. Commun.* 2013, **49**, 3784-3786; (b) I. Alkorta, J. Elguero, C. Roussel, *Comp. Theor. Chem.* 2011, **966**, 334-339; (c) G. Corongiu, P. Nava, *Int. J. Quantum Chem.* 2003, **96**, 395-404; (d) A. Göller, U.-W. Grummt, *Chem. Phys. Lett.* 2000, **321**, 399-405; (e) S. T. Howard, *J. Am. Chem. Soc.* 1996, **118**, 10269-10274.
- K. M. Gardinier, R. G. Khoury, J.-M. Lehn, *Chem. Eur. J.* 2000, **6**, 4124-4131.
- J.-L. Schmitt, A.-M. Stadler, N. Kyritsakas, J.-M. Lehn, *Helv. Chim. Acta.* 2003, **86**, 1598-1624.
- (a) L. L. Lao, J.-L. Schmitt, J.-M. Lehn, *Chem. Eur. J.* 2010, **16**, 4903-4910; (b) J.-L. Schmitt, J.-M. Lehn, *Helv. Chim. Acta.* 2003, **86**, 3417-3426.
- (a) M. N. Chaur, D. Collado, J.-M. Lehn, *Chem. Eur. J.* 2011, **17**, 248-258; (b) N. Parizel, J. Ramirez, C. Burg, S. Choua, M. Bernard, S. Gambarelli, V. Maurel, L. Brelot, J.-M. Lehn, P. Turek, A.-M. Stadler, *Chem. Commun.* 2011, **47**, 10951-10953; (c) A. R. Stefankiewicz, J. Harrowfield, A. Madalan, K. Rissanen, A. N. Sobolev, J.-M. Lehn, *Dalton. Trans.* 2011, **40**, 12320-12332; (d) M. Barboiu, M. Ruben, G. Blasen, N. Kyritsakas, E. Chacko, M. Dutta, O. Radekovich, K. Lenton, D. J. R. Brook, J.-M. Lehn, *Eur. J. Inorg. Chem.* 2006, 784-792; (e) N. Giuseppone, J.-L. Schmitt, J.-M. Lehn, *J. Am. Chem. Soc.* 2006, **128**, 16748-16763; (f) L. H. Uppadine, J.-M. Lehn, *Angew. Chem. Int. Ed.* 2004, **43**, 240-243.
- A. Coskun, M. Banaszak, R. D. Astumian, J. F. Stoddart, B. A. Grzybowski, *Chem. Soc. Rev.* 2012, **41**, 19-30.
- (a) C. J. Burns, J. F. Stoddart, *Nat. Nanotechnol.* 2013, **8**, 9-10; (b) K. Ariga, T. Mori, J. P. Hill, *Adv. Mater.* 2012, **24**, 158-176; (c) E. R. Kay, D. A. Leigh, F. Zerbotto, *Angew. Chem. Int. Ed.* 2007, **46**, 72-191.
- (a) K. Iseda, K. Kokado, K. Sada, *Reactive and Functional Polymers*, 2013, **73**, 951-957; (b) Y. Takashima, S. Hatanka, M. Otsubo, M. Nakahata, T. Kakuta, A. Hashidzume, H. Yamaguchi, A. Harada, *Nat. Commun.* 2013, **3**, 1270-1278; (c) J. Wei, Y. Yu, *Soft Matter*, 2012, **8**, 8050-8059; (d) R. Yoshida, *Adv. Mater.* 2010, **22**, 3463-3483; (e) H.-J. Schneider, R. M. Strongin, *Acc. Chem. Rev.* 2009, **42**, 1489-1500; (f) A. Didorenki, T. Krupenkin, A. Taylor, P. Tratzl, J. Aizenberg, *Science*, 2007, **315**, 487-490.
- (a) T. F. Otero, *J. Mater. Chem.* 2009, **19**, 681-689; (b) R. H. Baughman, *Science*, 2005, **308**, 63-35; (c) Z. Hu, X. Zhang, Y. Li, *Science*, 1995, **269**, 525-527; (d) Y. Osada, H. Okuzaki, H. Hori, *Nature*, 1992, **355**, 242-244.
- (a) L. Ionov, N. Houbenov, A. Sidorenko, M. Stamm, S. Minko, *Adv. Funct. Mater.* 2006, **16**, 1153-1160; (b) M. J. Bassetti, A. N. Chatterjee, N. R. Aluru, D. J. Beebe, *J. Microelectromech. Syst.* 2005, **14**, 1198-1207; (c) D. J. Beebe, J. S. Moore, J. M. Bauer, Q. Yu, R. H. Liu, C. Devadoss, B. H. Jo, *Nature*, 2000, **404**, 588-590.
- D. J. Hutchinson, S. A. Cameron, L. R. Hanton, S. C. Moratti, *Inorg. Chem.* 2012, **51**, 5070-5081.
- D. J. Hutchinson, L. R. Hanton, S. C. Moratti, *Inorg. Chem.* 2011, **50**, 7637-7649.
- D. J. Hutchinson, L. R. Hanton, S. C. Moratti, *Inorg. Chem.* 2010, **49**, 5923-5934.
- D. J. Hutchinson, L. R. Hanton, S. C. Moratti, *Inorg. Chem.* 2013, **52**, 2716-2728.
- (a) N. Giuseppone, J.-L. Schmitt, L. Allouche, J.-M. Lehn, *Angew. Chem. Int. Ed.* 2008, **47**, 2235-2239; (b) N. Giuseppone, J.-L. Schmitt, J.-M. Lehn, *J. Am. Chem. Soc.* 2006, **128**, 16748-16763.
- M. Barboiu, G. Vaughan, R. Graff, J.-M. Lehn, *J. Am. Chem. Soc.* 2003, **125**, 10257-10265.
- M. Barboiu, G. Vaughan, N. Kyritsakas, J.-M. Lehn, *Chem. Eur. J.* 2003, **9**, 763-769.
- J. Kuwabara, D. Takeuchi, K. Osakada, *Chem. Commun.* 2006, 3815-3817.
- (a) B. J. Hathaway, *Dalton. Trans.* 1972, 1196-1199. (b) B. J. Hathaway, in *Comprehensive Coordination Chemistry: The synthesis, reactions, properties & applications of coordination compounds*, ed. G. Wilkinson, R. Gillard, J. A. McCleverty, Pergamon Press, Oxford, 1987, vol 5, ch 53, pp. 652-688.
- (a) V. J. Argyle, L. A. Woods, M. Roxburgh, L. R. Hanton, *CrytEngComm*, 2013, **15**, 120-124; (b) A. G. Young, L. R. Hanton, *Coord. Chem. Rev.* 2008, **252**, 1346-1386; (c) A. J. Blake, N. R. Champness, P. Hubberstey, W. S. Li, M. A. Withersby, M. Schröder, *Coord. Chem. Rev.* 1999, **183**, 117-138.
- A.-M. Stadler, N. Kyritsakas, G. Vaughan, J.-M. Lehn, *Chem. Eur. J.* 2007, **13**, 59-68.
- (a) J. Harrowfield, *Helv. Chim. Acta.* 2005, **88**, 2430-2432; (b) L. Shimon-Livny, J. P. Glusker, C. W. Bock, *Inorg. Chem.* 1998, **37**, 1853-1867.
- (a) L. N. Dawe, K. V. Shuvaev, L. K. Thompson, *Chem. Soc. Rev.* 2009, **38**, 2334-2359; (b) A.-M. Stadler, *Eur. J. Inorg. Chem.* 2009, 4751-4770; (c) M. Ruben, J. Rojo, F. J. Romero-Salguero, L. H. Uppadine, J.-M. Lehn, *Angew. Chem. Int. Ed.* 2004, **43**, 3644-3662.
- A. W. Addison, T. N. Rao, J. Reedijk, J. van Rijn, G. C. Verschoor, *Dalton. Trans.* 1984, 1349-1356.
- L. Yang, D. R. Powell, R. P. Houser, *Dalton. Trans.* 2007, 955-964.
- N. M. Shavaleev, R. Scopelliti, F. Gumy, J.-C. G. Büzli, *Inorg. Chem.* 2009, **48**, 6178-6191.
- D. J. Hutchinson, L. R. Hanton, S. C. Moratti, *Acta. Crystallogr. Sect. E: Struct. Rep. Online*, 2009, **E65**, o1546.

- 32 C. A. C. Haley, R. Maitland, *J. Am. Chem. Soc.* 1951, 3155-3174.
- 33 X.-Y. Cao, J. Harrowfield, J. Nitschke, J. Ramírez, A.-M. Stadler, N. Kyritsakas-Gruber, A. Madalan, K. Rissanen, L. Russo, G. Vaughan, J.-M. Lehn, *Eur. J. Inorg. Chem.* 2007, 2944-2965.
- 34 (a) Z. Otwinowski, W. Minor, in *Processing of X-Ray Diffraction Data Collected in Oscillation Mode, Methods in Enzymology, Molecular Crystallography, Part A*, ed. C. W. Carter, R. M. Sweet, Academic Press, New York, 1997, vol. 276, pp. 307-326; (b) SAINT V4, *Area Detector Control and Integration Software*, Siemens Analytical X-ray Systems Inc, Madison, 1996.
- 35 G. M. Sheldrick, *SADABS, Program for Absorption Correction*, University of Göttingen, Göttingen, Germany, 1997.
- 36 G. M. Sheldrick, *Acta. Crystallogr. Sect. A.* 1990, **46**, 467-473.
- 37 A. Altomare, M. C. Burla, M. Camalli, G. L. Cascarano, C. Giacovazzo, A. Guagliardi, A. G. G. Moliterni, G. Polidori, R. Spagna, *J. Appl. Cryst.* 1999, **32**, 115-119.
- 38 G. M. Sheldrick, *SHELXL-97, Program for the Solution of Crystal Structures*, University of Göttingen, Göttingen, Germany, 1997.
- 39 L. J. Farrugia, *J. Appl. Crystallogr.* 1999, **32**, 837-838.
- 40 A. L. Spek, *Acta. Crystallogr. Sect. A.* 1990, **46**, 153-165.
- 41 (a) C. F. Macrae, P. R. Edgington, P. McCabe, E. Pidcock, G. P. Shields, R. Taylor, M. Towler, J. van de Streek, *J. Appl. Cryst.* 2006, **39**, 453-457; (b) I. J. Bruno, J. C. Cole, P. R. Edgington, M. K. Kessler, C. F. Macrae, P. McCabe, J. Pearson, R. Taylor, *Acta. Crystallogr. Sect. B.* 2002, **58**, 389-397.

Graphical Abstract

for

Tetratopic Pyrimidine-Hydrazone Ligands Modified with Terminal Hydroxymethyl and Acryloyl Arms and their Pb(II), Zn(II), Cu(II) and Ag(I) Complexes

Tetratopic pym-hyz strands with terminal hydroxymethyl (**L1**) and acryloyl groups (**L2**) were synthesized, characterized and reacted with Pb(II), Zn(II), Cu(II) and Ag(I) ions resulting in new linear, horse-shoe shaped and double helical complexes.

